The history of ground ice formation and intra-permafrost fluid flow as documented by Ra and Th isotopes

Dotan Rotem[1], Yishai Weinstein[1], Yehudit Harlavan[3], Adi Torfstein[4,5], Hanne H. Christiansen[2]

[1]Department of Environment, Planning and Sustainability, Bar-Ilan University, Ramat-Gan, 529002, Israel.

[2]Department of Environmental Science, Aarhus University, Denmark..
[3]Geological Survey of Israel, 32 Yesha'yahu Leibowitz, Jerusalem 9692100, Israel.
[4]Institute of Earth Sciences, Hebrew University of Jerusalem, Jerusalem, Israel.
[5]The Interuniversity Institute for Marine Sciences, Eilat, Israel.

Corresponding to: Dotan Rotem dotanrotem1969@gmail.com

Abstract

While permafrost is considered a permanently frozen soil, it often demonstrates evidence for internal processes, including fluid migration. Here, we present data of the chemistry, Ra, Th, and Ac isotopes of saline permafrost from three closely-retrieved cores drilled at Adventdalen, a fjord Valley in central Svalbard, which provides evidence for a fingering--style intra-permafrost fluid flow. Ground ice of the different cores differs markedly in their salinity and composition. In one core, which has a composition similar to seawater, the long to short-lived isotope ratios, $(^{226}Ra/^{223}Ra)_{AR}$ and $(^{226}Ra/^{224}Ra)_{AR}$, are relatively low, being similar to parent isotope activity ratios ($^{230}Th/^{227}Ac$ and $^{230}Th/^{228}Th$, respectively) on grain surfaces (CEC exchangableexchangeable fraction). Ground ice of the two other cores, which are less saline and have Na/Cl and SO_4/Cl ratios higher than seawater, demonstrates much higher Ra isotope ratios, closer to parent ratios in the bulk sediment. It is suggested that the different isotope ratios are due to different residence times, and that the parameter controlling the isotope ratios is radium diffusion from inside the grains, probably via frozen nano-pores. While ground ice in the less saline cores was formed during permafrost formation (10-9 ka), ground ice average residence time in the more saline core is shorter, <<2,000 years, which did not allow a significant diffusion of the long-lived ^{226}Ra from inside the grains. The latter is probably the result of a Late Holocene intrusion of and mixing with saline fluids, arriving from a low-Th or high water:rock ratio basement rock. Recent salinization is also supported by the presence of high salinity also in the syngenetic permafrost, which has been deposited 4-2 ka. This The above highlights the internal dynamics of saline permafrost, which may affect its resilience to the ongoing global warming.

1. Introduction

Permafrost is a soil or rock that has remained at or below 0 °C for at least two consecutive years. While permafrost covers more than 20% of the northern hemisphere land area, it is evident that its distribution has dramatically declined during the last several decades, due to the ongoing global warming (Brown et al., 2002; Obu et al., 2019; Li et al., 2022), with continuous permafrost areas changing into discontinuous and sporadic permafrost zones (Kwong and Gan, 1994; Anisimov and Nelson, 1997; Osterkamp and Romanovsky, 1998; James et al., 2013). While some of the permafrost is very old and thick, in particular in inland settings, such as Siberia, Canada, Alaska, and Antarctica (Gilichinsky and Wagener, 1995; Dobinski, 2011; Abramov et al., 2021), other areas are dominated by young permafrost (Late Pleistocene to Holocene), related to the last deglaciation, which exposed vast areas to the atmosphere and opened the way for cooling and permafrost formation (e.g., Jin et al., 2007; French, 2007). Following exposure, permafrost aggradation may go two ways. The first, applied to the already deposited sediments and bedrock, is the top-down, epigenetic permafrost formation, while the other is the bottom-up, syngenetic cooling and freezing of the newly deposited sediments.

Whereas most permafrost is significantly colder than 0ºC, it is not necessarily strictly frozen (French, 2007; Dobinski, 2011; Keating et al., 2018), which is due to both the lowering of the freezing point in saline permafrost (Ahonen, 2001), as well as due to capillary or surface adsorption effects in the sediment pore space (e.g., Sheshukov and Nieber, 2011; Wang et al., 2020), which in turn could be related to water content and grain size (e.g., Zhang et al., 2018; Wang et al., 2021). The presence of fluids may boost intra-permafrost processes, allowing the re-distribution and migration of fluids in the cryotic pore space (Fisher et al., 2019; Lacelle et al., 2022). Intra-permafrost processes are often associated with supra-permafrost processes, such as infiltration from the active layer (Mackay, 1983; Marsh and Woo, 1993; Boike et al., 1998), runoff on slopes to form foothill mounds (Åkerman and Malmström, 1986), intrusion from rivers (Alekseyev, 2015) and thaw-freeze crack-filling, which produce the commonly-observed ice wedges and polygon structures (e.g., Harry and Gozdzik, 1988; Mackay, 1989; Christiansen et al., 2005; Opel et al., 2018). On the other hand, intra-permafrost ice segregation is also common (Mackay, 1983; Mackay and Dallimore, 1992; Solomatin and Xu, 1994; Fu et al., 2022; Kipp et al., 2025). While this is more difficult to trace, Weinstein et al., (2019) showed by Ra and Th isotopes, combined with ^3H, that a segregated ice layer at Adventdalen, central Svalbard (Fig. 1), had been formed very recently (less than one year).

Naturally, due to its lower freezing temperature, saline permafrost (i.e., soils with significant content of soluble salts, such that results in a freezing point depression, e.g., Banin and Anderson, 1974; Marion, 1995) is more prone to fluid migration and intra-permafrost processes. Near-surface saline permafrost is widely distributed in the northern circumpolar region, especially in the continuous permafrost zone, covering up to 35% of that area (Brouchkov, 2002). The salinity source is commonly related to seawater (Hivon and Sego, 1993; Brigham-Grette and Hopkins, 1995; Forman et al., 2004; Lønne and Nemec, 2004; Jones et al., 2023), although it can also be strictly terrestrial, related to evaporation processes in inland basins and to water-rock interaction (e.g., Dickinson and Rosen, 2003; Henkemans, 2016; Gao et al., 2017). Salinity and cryotic state (i.e., freezing degree of the pore fluid) are highly heterogeneous in the saline permafrost environment (e.g., Brouchkov, 2002; Ahonen, 2001; Dafflon et al., 2016). This heterogeneity is sometimes manifested by the presence of lenses of unfrozen ground or overcooled brines ('cryopegs'), which usually form due to freezing and salt expulsion processes (e.g., Yershov, 1998; Iwahana et al., 2021).

In Svalbard, near-surface saline permafrost is commonly observed in fjord valleys, where seawater ingression occurred during the early Holocene, following glacial retreat and sea level rise (e.g., Cable et al., 2018; Gilbert et al., 2019; Rotem et al., 2023). Permafrost formation ~~has~~ had been inhibited until after seawater regression and the exposure of the recently deposited sediments to the atmosphere (Gilbert et al., 2018). The actual formation of the permafrost depends on the combination of climatic and soil physical attributes. Accordingly, while Hornum et al., (2020) argued that freezing at Adventdalen (Fig. 1) did not occur until 4500 years BP due to the relatively warm mid-Holocene, Rotem et al., (2023) suggested that permafrost started forming immediately after exposure (ca. 9 ka), which was assisted by the thermal conductivity difference between solid ice and liquid water. In this paper, we show by chemistry and radioisotopes that the permafrost in eastern Adventdalen demonstrates a complex and multi-stage history of ground ice formation.

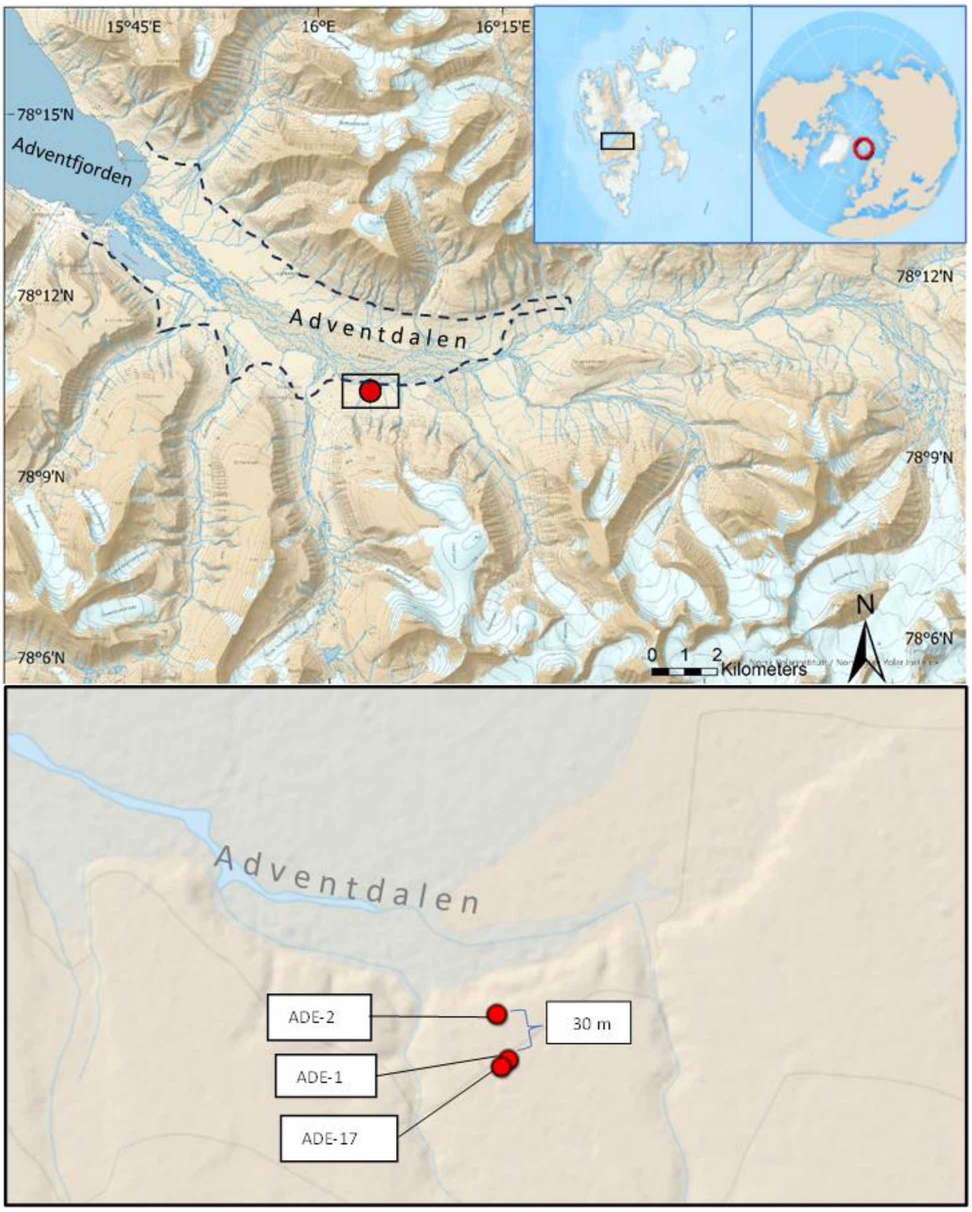

Figure 1: Location and detailed map of the ADE study site. The dashed line represents sea ingression limit at the early Holocene (Lønne and Nemec, 2004, drawn after Hodson et al., 2020). The map is provided with courtesy of the Norwegian Polar Institute.

1.1 Radium isotopes

In this work, we report the activities (disintegrations per time) ~~(i.e., concentrations)~~ of radium isotopes in ground ice, as well as their radioactive parents (thorium and actinium) on the permafrost sediments. Radium has four naturally occurring isotopes: ^{223}Ra, ^{224}Ra, ^{226}Ra, and ^{228}Ra. All isotopes are produced by decay chains, stemming from ^{238}U, ^{235}U, and ^{232}Th (Fig. 2). Specifically, all Ra isotopes are produced by the α decay of different Th (thorium) isotopes (^{227}Th, ^{228}Th, ^{230}Th and ^{227}Th, respectively). , although Iin the case of ^{223}Ra, we mainly usually relate to its grandparent 'grandparent' ^{227}Ac with a half-life of 21.772 years, due to the short life of its direct parent ^{227}Th (half-life: 18.7 days). An important aspect is that chemically, tThorium (parent isotope) is highly particle-reactive and tends to strongly adsorb ons to mineral surfaces, whereas rRadium acts as a is more mobile and is more common in the alkaline earth metal that prefers the dissolved phase. PhysicallyAlso, the alpha-recoil effect during radioactive decay provides the kinetic energy necessary to eject rRadium from the mineral lattice into the pore waterspace. while thorium (parent isotopes) is a particle-reactive element (i.e., in the presence of water, it will always be on the solids), radium is much more mobile in water. The ^{226}Ra is the longest-lived radium isotope, with a half-life of 1601 years, ; ^{228}Ra has a half-life of 5.8 75 years, while ^{224}Ra and ^{223}Ra are short-lived, with half-lives of 3.66 and 11.4 days, respectively. (Bourdon et al., 2003). The wide range of half-lives of the radium isotopes allows their application to various processes with very different time scales. For example, for short-term groundwater processes, ^{228}Ra, ^{223}Ra, or ^{224}Ra, and their activity ratios are good tracers (e.g., Moore, 2003; Hsieh et al., 2013). However, for a distinction between thawed ground ice and active layer water or between young and old sub-permafrost groundwater, ^{226}Ra would be a better tracer, since its growth toward equilibrium with its parent nuclide, ^{230}Th, takes 5-6 half-lives (8-10,000 years; e.g., Weinstein et al., 2019; Rotem et al., 2024).

Radium isotope research in the polar regions has been mostly focused on the land-ocean interface, like shelf-deep basin exchange processes (Rutgers van der Loeff et al., 1994; Kipp et al., 2019, 2023), river discharge as a carrier of carbon and nutrients to the oceans (Rutgers van der Loeff et al., 2002; Bullock et al., 2022) or lakes (Dabrowski, 2020) and direct groundwater discharge to the sea (e.g., Dimova et al., 2015; Charkin et al., 2020). While also studied in relation to soil or river contamination (e.g., Chevychelov and Sobakin, 2017), as tracers of weathering processes (Linhoff et al., 2020), or as part of geological and pedological surveys (e.g., Wojtasik et al., 2017), radium isotopes have just recently been studied as a potential tracer of permafrost degradation-segregation or as a proxy for residence time determination (Weinstein et al., 2019; Kipp et al., 2025). In fact, the only radioisotopes that were used for the determination of ground ice residence time in permafrost soil were uranium isotopes (Ewing et al., 2015) and ^{3}H (for young ice, e.g., Burn and Michel, 1988).

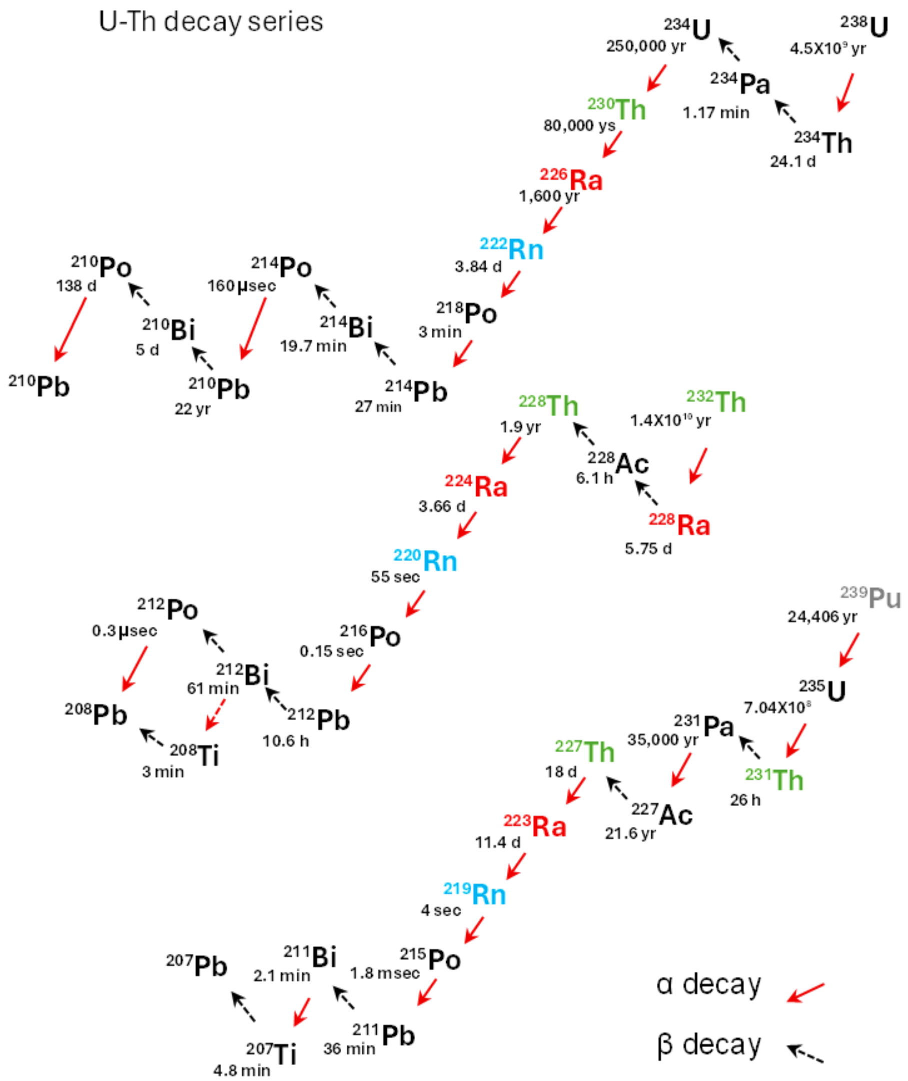

Figure 2: The three U-Th decay series. Radium isotopes are designated red, and Thorium is labelled green. Note that all Ra isotopes are produced by ~~a~~ the decay of Th isotopes, and that two of the four Ra isotopes are along the ^{232}Th decay chain.

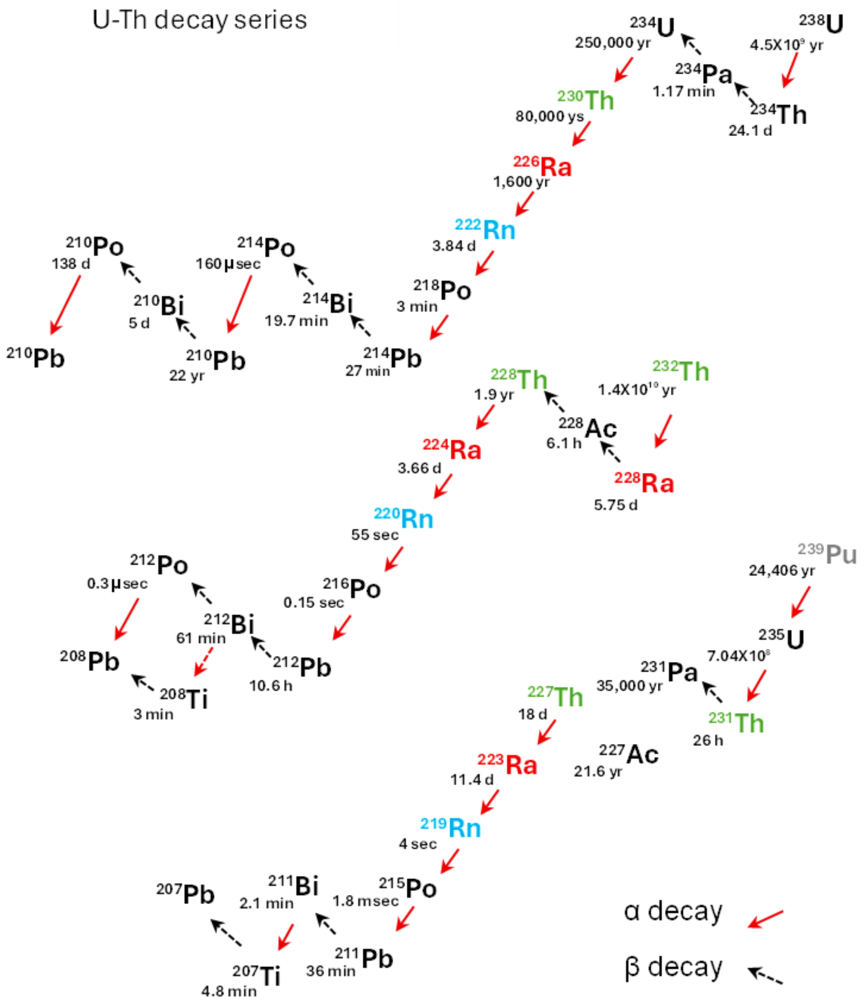

~~Figure 2: The three U-Th decay series. Radium isotopes are designated red and Thorium is labelled green. Note that all Ra isotopes are produced by a decay of Th isotopes, and that two of the four Ra isotopes are along the ^{232}Th decay chain.~~

2. Study site

The data presented in this study are from cores drilled into the permafrost in the Adventdalen Valley (hereafter Adventdalen), Svalbard (Fig. 1), during March 2017 and March 2022. The Adventdalen is a U-shaped fjord valley, carved by advancing and retreating glaciers. During the last glacial cycle, it was eroded to its basement (Elverhøi et al., 1994), which was followed by Early Holocene glacier retreat and seawater ingression up valley (Lønne and Nemec 2004), resulting in the deposition of deltaic sediments (Gilbert et al., 2018). A relatively fast elastic rebound (Forman et al., 2004) resulted in the exposure of the sediments to the atmosphere, starting at the eastern part of the valley ca. 9.5 ka and arriving at the current coastline location no later than 4 ka (Gilbert et al., 2018). The exposed sediments froze epigenetically within a short time after exposure to the atmosphere (100s years; Rotem et al., 2023). The marine sediments were then covered by several meters of mid to Late Holocene fluviatile sediments, which were overlain by 2-3 m of aeolian deposits, and both went through syngenetic freezing (Gilbert et al., 2018). At present, the thickness of the permafrost in the valley is estimated at less than 100 m next to the coast (Humlum et al., 2003) and up to 250 m up-valley (Isaksen et al., 2001), most of it being epigenetic and the shallow 4-5 m syngenetic, while active layer depth ranges between 0.5-1 m (Christiansen et al., 2005; Weinstein et al., 2019). Permafrost in Svalbard is considered continuous (Obu et al., 2019), although non-frozen and partially frozen permafrost were also reported (Keating et al., 2018; Weinstein et al., 2019), and recent works about sub-permafrost hydrology also question the continuity of the permafrost in this area (e.g., Rotem et al., 2024).

Four boreholes were drilled at the ADE site -, a river terrace, 23 m.a.s.l, 9.8 km up-valley from the Adventfjorden (Fig. 1). Two closely spaced (0.5 m apart) boreholes, centered at 78.17220N 16.06130E, were drilled during spring 2017, and they are treated here as one core, ADE-17. The other two cores, ADE-1 and ADE-2, were drilled in spring 2022. ADE-1 is located within a few meters from ADE-17 (78.17216N 16.0610E) and ADE-2 was drilled ca. 30 m away (78.17243170N 16.06114840E). The valley-fill section at the site (14-20 m, Gilbert et al., 2018 and this study) consists of 1.5 m of fine-grained aeolian deposits underlain by fluviatile gravel down to 5.5 m, which in turn is underlain by deltaic sediments (ca. 12 m). The Holocene section covers glacial sand deposits, 2.5 m thick (Gilbert et al., 2018), which are underlain by basement rocks (Lower Cretaceous, shales) (Grundvåg et al., 2019).

3. Methods

The drilling campaigns were executed using the University Center in Svalbard (UNIS) permafrost drill rig (Gilbert et al., 2018), using core barrels of 43 mm diameter (ID) in 2017 and 58 mm in 2022. The two boreholes drilled in 2017 reached depths of 13 and 9 m, while the 2022 ones (ADE-1 and -2) reached a depth of 16 m. In the latter, the bottom 1-2 m was composed of bedrock, which was excluded from sample processing. The upper 5 m (syngenetic part) of ADE-2 was drilled with a jackhammer and,. While the extracted cuttings have beenwere analyzed only for chemistry (no Ra isotopes), the results are not presented in this study due to possible downhole contamination. Core length, borehole depth, core freezing status, and gravel content were recorded in the field. Retrieved core sections were sealed in plastic bags and stored frozen at −18 °C at UNIS. The cores were subsequently sectioned in a cold room (−5 °C) into 0.5–1 m depth-intervals. Subsamples were scraped and crushed into small fragments, which were transferred to 250 ml centrifuge tubes. For samples with low water (ice) content, up to 40 ml of Ra-free water was added to facilitate porewater extraction. The samples were then thawed in a microwave oven at 600 W for 2 min and centrifuged for 8 min at 11,000 rpm (high g) to separate the meltwater from the soil matrix. The extracted water was sequentially filtered through 3 µm and 0.45 µm. Net water volumes extracted varied strongly (in accordance with the high variability of ice content) and summed to 42-1391 ml per sample. It is important to note that in this paper, we consider all extracted water as thawed ground ice, although some of the core segments were not fully frozen, thus liquid water could also be present to a certain amount, especially in the more saline samples (see Keating et al., 2018; Weinstein et al., 2019). We also note that the mentionedcentrifuging, as well as the addition of Ra-free water to samples with low ice content, could result in some desorption from grain surfaces, as well as in salt dissolution when exists. Yet, both salts and adsorbed ions are assumed part of the pore space chemistry (see a similar conception by Ewing et al., 2015, regarding U isotopes in ground ice). Nevertheless, the discussion in this study focuses on Ra isotope ratios, which isare less affected by possible desorption. Please also see the discussion of $(^{224}Ra/^{228}Ra)_{AR}$ in section 5.4..

Most of the extracted water was used for Ra isotope analysis, while 30-60 ml was used for elemental chemistry analyses. For Ra isotopes, the solution was run at least three times through columns, filled with 20 g manganese-coated fibers (flow rate of 0.5 l/min). Samples with pH lower than 6 were pre-treated by adding a low

~~concentration~~low-concentration NaOH solution (Ra-free). Sample water was also run through a secondary ~~, 20 g,~~ Mn-coated fiber to account for Ra adsorption efficiency. In six samples (DR-AD-121-126), the adsorption efficiency was determined by measuring and comparing ^{226}Ra on both fibers and water samples. Efficiencies were very variable, from 90% down to <50%, with the lower end being ~~probably~~ mainly due to the relatively low pH and/or reducing conditions~~, and in certain samples due to high salinity.~~. Measured activities of all isotopes were corrected accordingly, assuming no mass-dependent fractionation. Nevertheless, due to the uncertainties about both extraction protocol and adsorption efficiency on the fibers, in this paper, we mainly focus on isotope ratios.

The short-lived ^{224}Ra, and ^{223}Ra were measured by the RaDeCC system (Moore and Arnold, 1996) within 2-3 days after water-soil separation, while ^{223}Ra was also measured after ca. 10 days, as to check for 220-219 cross-talk interferences (e.g., Diego-Feliu et al., 2020). We note that we found no evidence for cross-talk (i.e. time-corrected activities showed no higher activities during the first compared with the later measurement), which is probably due to the low activities of both isotopes (^{224}Ra was mostly <0.5 cpm). Both ^{224}Ra and ^{223}Ra were corrected for chance coincidence, following Moore and Arnold (1996). ~~was measured by the RaDeCC system (Moore and Arnold, 1996) within 2-3 days after water-soil separation, while ^{223}Ra was measured after ca. 10 days, as to minimize the cross-talk between ^{224}Ra and ^{223}Ra.~~ ^{224}Ra was re-measured after 3-4 weeks, after reaching equilibrium with its radioactive parent ^{228}Th. Fibers were measured for ^{226}Ra by an emanation system and Lucas Cells (Mathieu et al., 1988) after a 3-week incubation, to allow for ^{222}Rn equilibration with ^{226}Ra. ^{228}Ra was measured by a ~~low background~~low-background well-type HPGe gamma spectrometer (Canberra), using the 911 KeV peak of ^{228}Ac. All results are presented as dpm (disintegrations per minute) per liter of thawed ground ice, which can change strongly due to the ice content of the permafrost. Analytical errors on ^{226}Ra, ^{228}Ra~~,~~ were ≤7%, while on ~~and~~ ^{224}Ra they were ~~commonly~~ ≤~~10~~13%, ~~while~~ and those ~~of~~ on the low activity ^{223}Ra ~~were~~ averaged 28%, and in ~~certain~~ two cases ~~up to >~~exceeded 4~~3~~0% (errors ~~Weinstein et al., 2019~~determined, following the protocol of Garcia-Solsona et al. 2008).

The Radium isotopes accumulate in the frozen pore space following recoil from their parent nuclides Th and Ac, which are mostly located either on or within the sediment grains. Accordingly, thorium isotopes and ^{227}Ac were measured both in the bulk grains and in the ~~adsorbed~~ exchangeable fraction of the permafrost sediment, after thawing and completing the ground ice-soil separation. Several grams of soil samples were disaggregated and homogenized in an agate mortar for the bulk sediment analysis. For the bulk sediment measurements, 0.3 g of each sample was placed in a Teflon beaker and was treated with 1 ml HF and 5 ml HNO_3 (both concentrated, ultrapure grade). A droplet (ca. 0.035 ml) of a ^{229}Th spike (86 ppt) was added to the solution, and the beakers were placed on a hot plate (200 ^{0}C) to let evaporate. The residue was then treated with 5 ~~ml~~ mL HCl. A few drops of H_2O_2 were added to treat the organic matter content. The solution was evaporated, and the ~~sample was~~n dissolved ~~in~~by 6 mL 7 N HNO_3. ~~2~~Two ml~~L~~ (out of the 6), dedicated for ^{232}Th and ^{230}Th analyses, were run ~~via~~through Bio-Rad AG 1X8 200-400 mesh resin, following the protocol for t~~T~~horium ion chromatography separation (Grant et al., 2012). The remaining fraction of 4 ml was buffered with NaOH to pH~7 and kept for ^{228}Th and ^{227}Ac analyses. The exchangeable fraction of thorium and actinium on grain surface was determined by the CEC (Cation Exchange Capacity) ammonium acetate leaching protocol (e.g., Sumner and Miller, 1996). Five grams of sediment was shaken with 25 mL ammonium acetate overnight. The sample was then centrifuged, and the liquid phase was evaporated, dissolved in 2 mL 7N HNO_3 and run through the Bio-Rad resin (above) for ^{232}Th and ^{230}Th analyses. A second set of 5 g sediment was prepared for ^{228}Th and ^{227}Ac, using the same protocol (albeit no chromatography).

^{230}Th and ^{232}Th (radioactive parents of ^{226}Ra and ^{228}Ra, respectively) were determined by athe Neptune Plus Multicollector ICPMS at the Institute of Earth Science, The Hebrew University of Jerusalem. The other 4 mL were buffered to pH ~7 using NaOH and passedAll samples for ^{228}Th and ^{227}Ac were run through 20 g manganese-coated fibers as described above. ^{228}Th and ^{227}Ac (parents of ^{224}Ra and ^{223}Ra, respectively) were studiedand measured by the RaDeCC system (Moore and Arnold, 1996), assuming equilibrium has been achieved with their short-lived radium isotope daughters. The adsorbed exchangeablefraction was determined by the CEC (Cation Exchange Capacity) measuremento (Ref…). A 5 g sediment sample of each sample, was shaken with 25 mL of ammonium acetate for 16 hours. Sample The sample was then centrifuged, and the liquid phase was evaporated and dissolved in 2 mL 7 N HNO_3. ^{230}Th and ^{232}Th were determined following the abovementioned procedure. A second set of 5 g sediment samples was treated with ammonium acetate, shaken, and centrifuged, then buffered and run via 20 g manganese-coated fiber to determine ^{228}Th and ^{227}Ac. The final products of both protocols (bulk and CEC) were dissolved in 7 N HNO_3 (6 ml, and 2 ml, respectively). Solutions (2 ml) were run via Bio-Rad AG 1X8 200-400 mesh resin, following the protocol for Thorium ion chromatography separation (Grant et al., 2012). ^{230}Th and ^{232}Th (radioactive parents of ^{226}Ra and ^{228}Ra, respectively) were determined by a Neptune Plus Multicollector ICPMS at the Institute of Earth Science, The Hebrew University of Jerusalem. ^{228}Th and ^{227}Ac (parents of ^{224}Ra and ^{223}Ra, respectively) were studied separately by the RaDeCC system (Moore and Arnold, 1996), assuming equilibrium has been achieved with their short-lived radium isotope. Results are presented as dpm g^{-1} sediment. Analytical errors for the MC-ICPMS thorium measurements were up tobelow 2% and 0.5% for the bulk sediment and 0.5% for theand CECexchangeable fractions, respectively, while . In the RaDeCC measurements, while RaDeCC errors for ^{228}Th and ^{227}Ac were up to were <17% (average of 8%), and those of the ^{227}Ac averaged 23% for the exchangeable fraction and 34% for the bulk sediment, which is due to the low counts. Major elements were analyzed at the Geological Survey of Israel (GSI). Cations and SO_4^{-2} were measured by inductively coupled plasma atomic emission spectroscopy (ICP-OES; Optima 5300). The Cl^- concentrations were determined according to their concentration in the solutions; above 50 ppm via potentiometer titration (Metrohm 702 SM Titrino titrator connected to a chlorine electrode), or while below 50 ppm by Ion Chromatograph, which was also used for the Br^- concentrations. Bicarbonate was analyzed as alkalinity via titration (analyzed only in 60% of the samples). The analytical error for all majors is less than 5%. We note that the chemistry of ground ice in ADE-17 was already presented in Rotem et al., (2023). Ice content, defined as gravimetric moisture content (W–D)/D × 100, where W and D refer to the wet and dry sample mas mass (Gilbert et al., 2018).

4. Results

4.1. Ground-ice chemistry

Ice content (frozen water mass divided by dry mass) of the samples varied strongly, from 2% to >180% (180% ice content translates into 64% water content), and was, in general, higher in the shallow, syngenetic part (Table C1, Appendix A).

Ground-ice (i.e., water extracted from thawed permafrost) chemistry differs strongly between the cores and between the shallow, syngenetic and the deeper, epigenetic part of the permafrost profile. of the syngenetic section (In cores ADE-17 and ADE-1, chemistry of the syngenetic ground-ice) is basically that of fresh water with typical TDS concentrations of 100-200<400 mg l^{-1} (Table C1), while ionic ratios of major elements to Cl^- are higher than that of seawater»1 (e.g., Na/Cl of 1.01-3.58, Figs. 3 and 4). On the other hand, ground ice in the epigenetic section, deeper than 5-5.5m, is mostly brackish to saline, which varies between the cores. While in ADE-1 and ADE-17, Cl^- concentration is with 450-<2,400 and <3,700 230 mgCl^- l^{-1} (~4 to 12 PSUTDS of 900-6,500 mg l^{-1}; note that HCO_3^- and Mg^{2+} were not measured in some of the samples), respectively, . in In ADE-2, salinity it is significantly higher (up to 7,9600 mg Cl^- -l^{-1} and TDS of 17,190 mg l^{-1} (~14 PSU compared to 37 PSU in modern seawater salinity)), with one outlier (DR-AD-125 from ADE-2) reaching >23,000 as high as 22,732 mgCl^- l^{-1} and TDS of >14,33340,000 mgNa^+ l^{-1} (Table C1). While the higher salinities were observed at epigenetic depths (>5.5m), salinities in the syngenetic section of ADE-2 were also relatively high (TDS »1000 mg l^{-1}), which reached TDS concentrations >6000 mg l^{-1} at the base of this section (Table C1).

In ADE-17, Cl^- and other major elements show a mixing pattern with depth, with concentrations increasing from 438 470 mgCl l^{-1} at 5.56 m to 2,1501,900-3,200680 mgCl l^{-1} at 9-12 m (Figs. 3a-e). This is not observed in ADE-2, where high salinities are observed up to the top of the epigenetic section. Unlike Cl^-, the Ca^{+2} does not show any pattern with depth also in ADE-17, and concentrations in the epigenetic section are similar to those in the syngenetic one (Fig. 3f).

Ion ratios vary along the profilein the ground-ice of ADE-17 and ADE-1. vary stronglyWhile in the syngenetic part, with Na/Cl and SO_4/Cl are mostly much higher than in seawater (equivalent ratios showing up to 3.60 and 10.77, respectively, in the syngenetic section (Figs. 4 and 5a-b, no data for ADE-2), and lower ratios, in the epigenetic part, ratios are (≤2 and ≤0.45, respectively, (Figs. 5a-b). Nevertheless, in ADE-17 and ADE-1, ratios at the shallow part of the epigenetic section (6-10 m) are also relatively high (up to 1.92 and 0.45, respectively), showing a rough continuum with the deep part of the syngenetic section (Figs. 5a-b). On the other hand, in ADE-2 (epigenetic section) ratios are more uniform, with Na/Cl equivalent ratios similar to that of seawater (0.84-1.02) both in epigenetic and the syngenetic section (except for the shallowest-measured sample, at 3.5 m, with Na/Cl=0.4), and SO_4/Cl (in the epigenetic section) mostly lower than that of seawater (≤0.1, Figs. 4 and 5a-b). Ca/Cl, Mg/Cl, and K/Cl generally show similar patterns, with very high K/Cl and, to a lesser extent Ca/Cl in the syngenetic part, while close to seawater ratios in the epigenetic part of the profile, this time in all cores (except for the highly saline DR-AD-125, Figs. 5c-d; one outlier, with very high K and low Ca and Mg at 11m, ADE-2, which could be analytical).

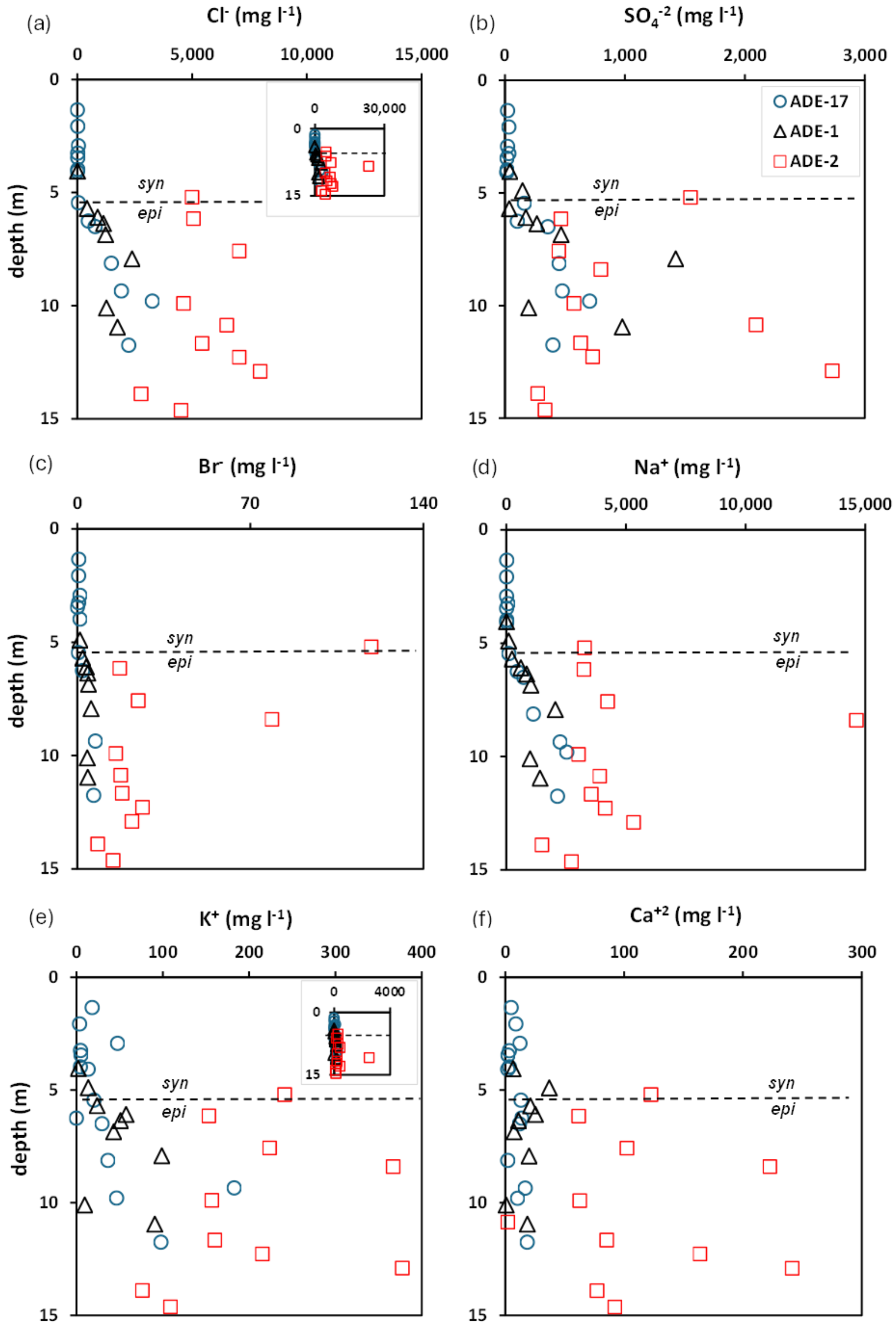

Figure 3: Concentration of selected major elements along the profile of the three ADE cores (ADE-17, ADE-1, and ADE-2). The dashed line shows the boundary between syngenetic *(syn)* and epigenetic *(epi)* permafrost at the site (Gilbert et al., 2018). The insets in the Cl^- and K^+ diagrams are for sample DR-AD-125 and DR-AD-150, respectively.

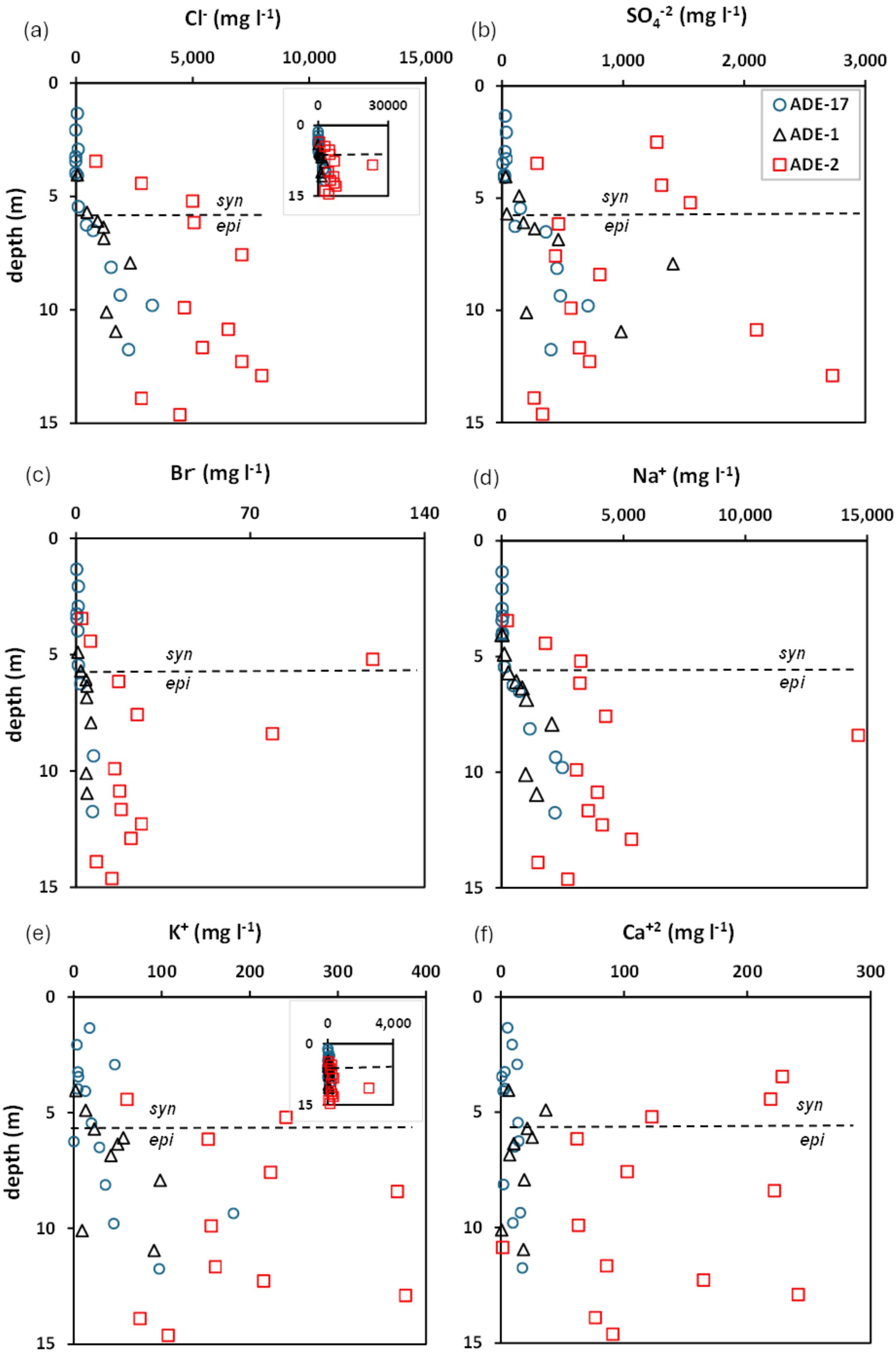

Figure 3: Concentration of selected major elements along the profile of the three ADE cores (ADE-17, ADE-1, and ADE-2). The dashed line shows the boundary between syngenetic *(syn)* and epigenetic *(epi)* permafrost at the site (Gilbert et al., 2018). The insets in the Cl^- and K^+ diagrams are for sample DR-AD-125 and DR-AD-150, respectively.

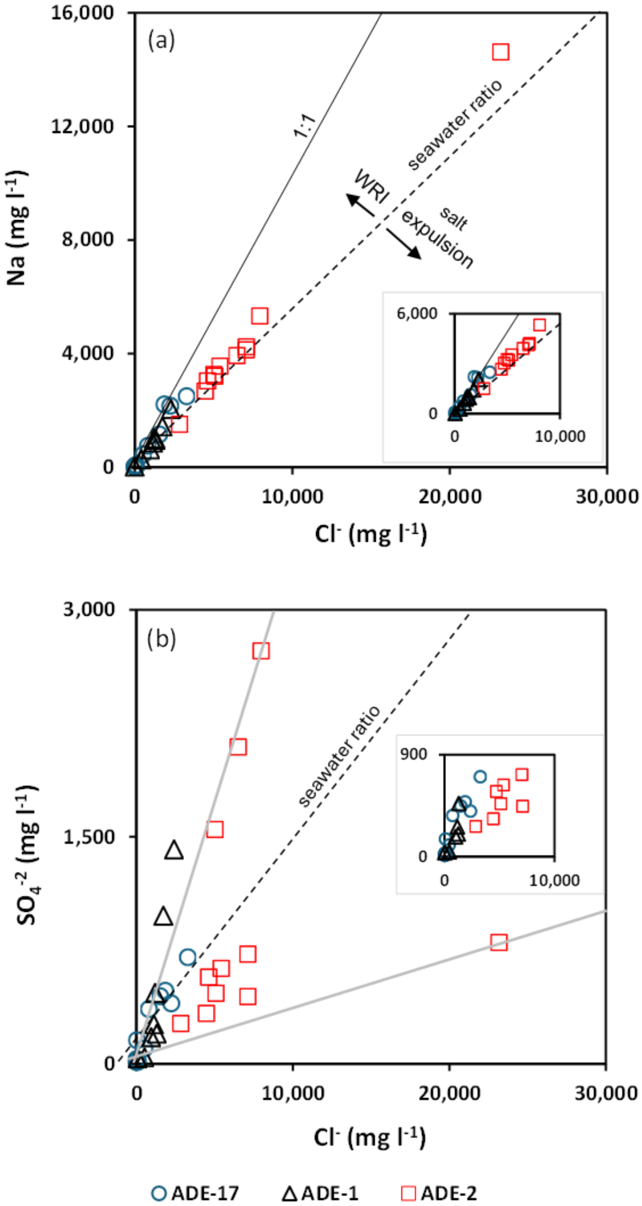

~~Figure 4: (a) Sodium and (b) sulphate against chloride in the ground ice of the ADE cores. WRI refers to Water-Rock Interaction.~~

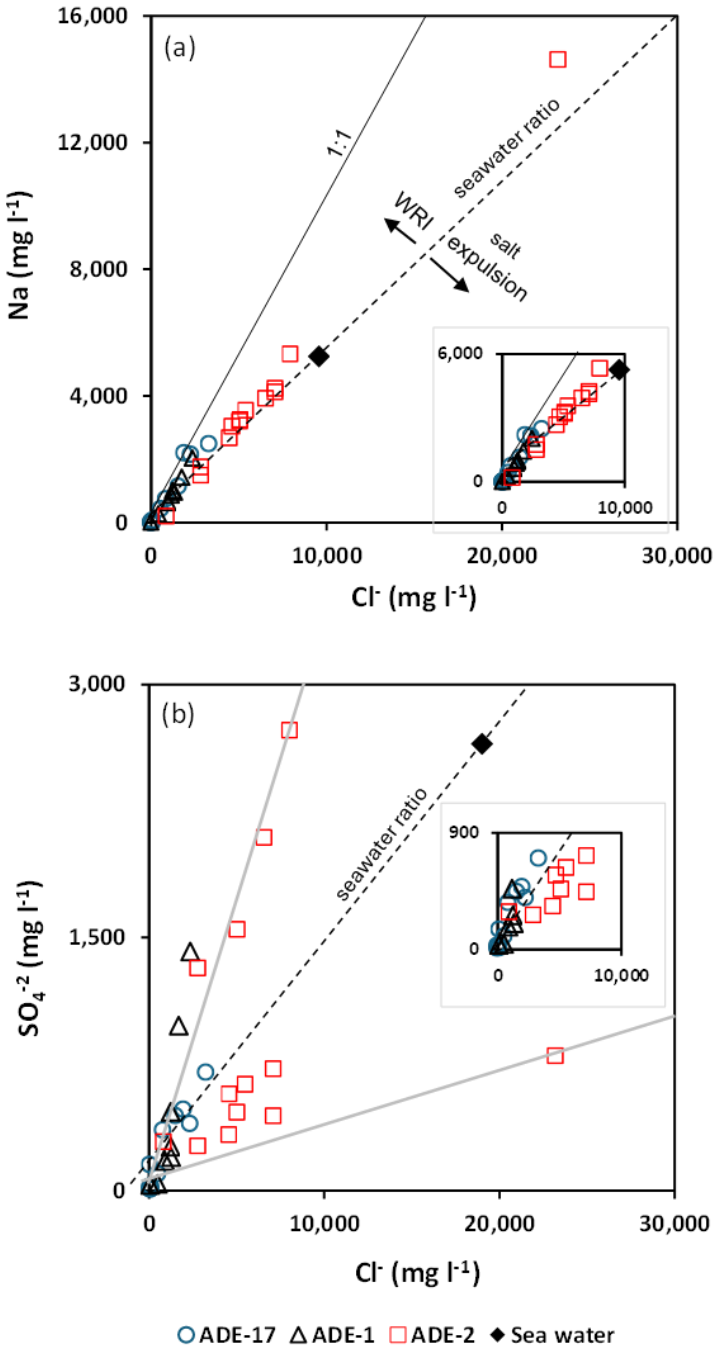

Figure 4: (a) Sodium and (b) sulphate against chloride in the ground ice of the ADE cores. WRI refers to Water-Rock Interaction.

350

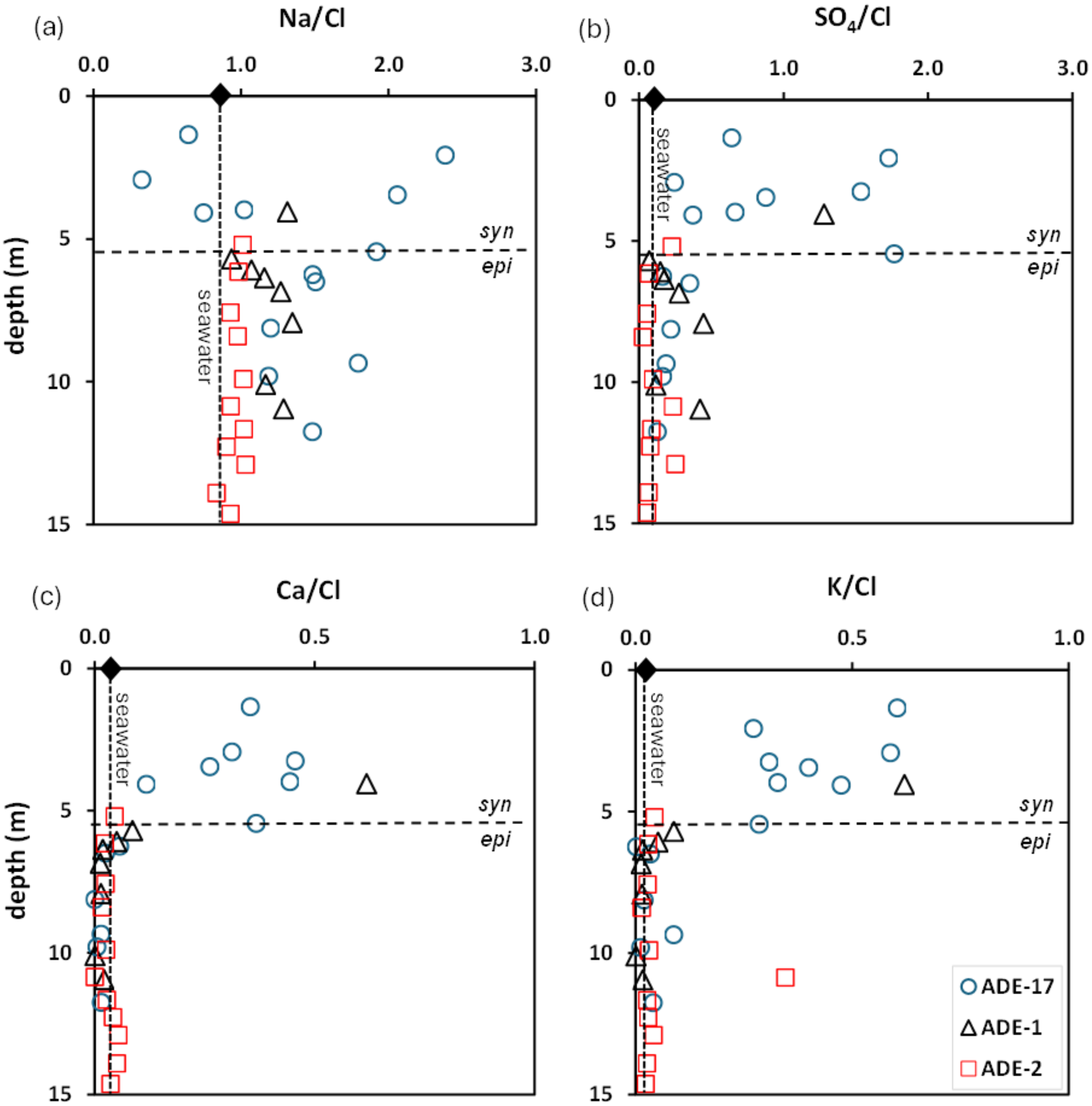

Figure 5: Ground ice equivalent ratios in the ADE cores. The black full diamond and vertical dashed line is for seawater composition (de Baar et al., 2017, Salinity of 35 ppt). The horizontal dashed line as in Figure 3.

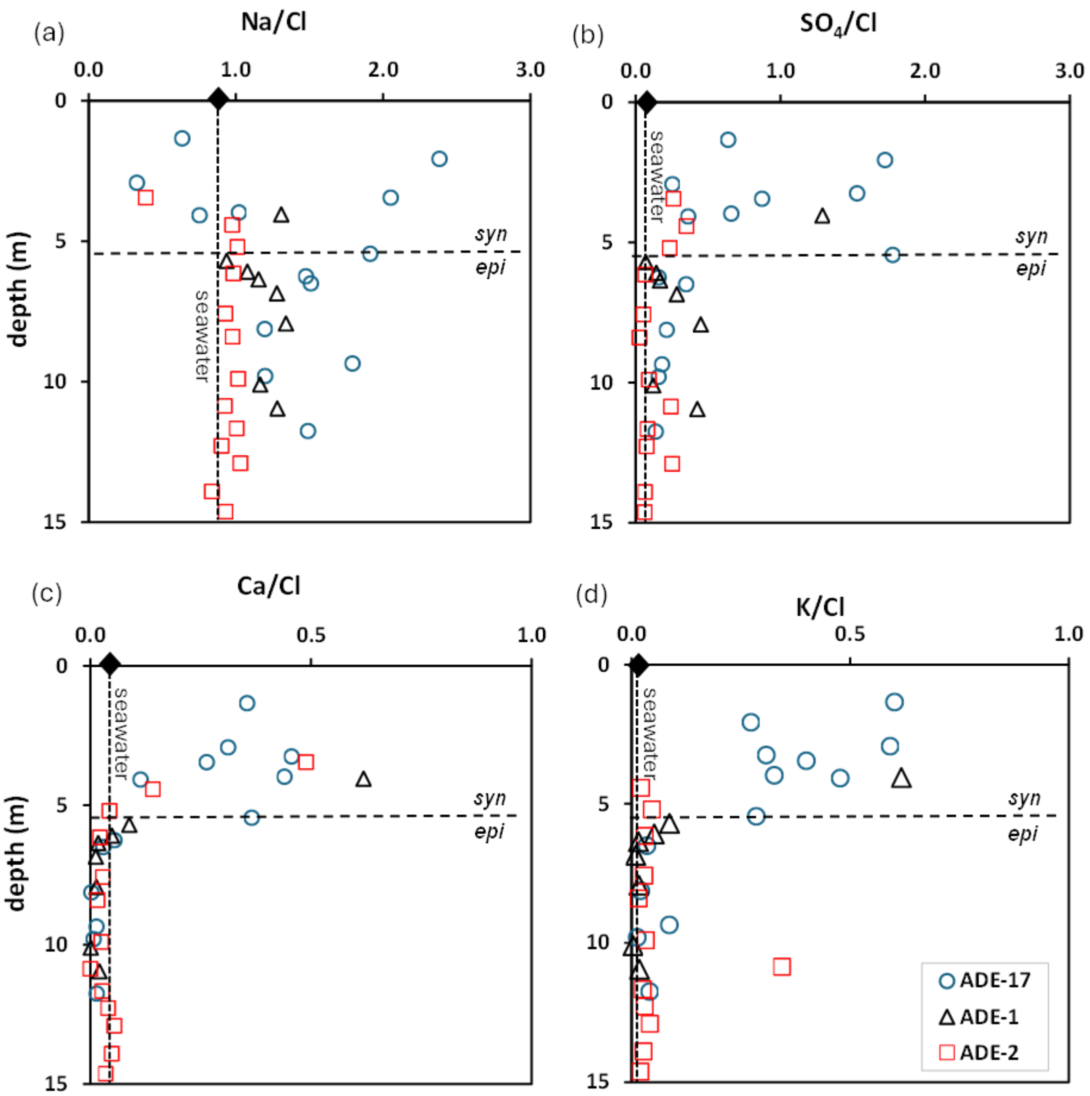

Figure 5: Ground ice equivalent ratios in the ADE cores. The black full diamond and vertical dashed line is for seawater composition (de Baar et al., 2017, Salinity of 35 ppt). The horizontal dashed line as in Figure 3.

4.2. **Radium isotopes in ground ice**

Radium isotope activities in ground-ice are presented in Table C2. Activities of ^{226}Ra, ^{228}Ra, and ^{224}Ra in ground ice are quite similar, varying between <1 to 60 dpm l^{-1} (averages of 10-13 dpm l^{-1}), while ^{223}Ra ~~is an order of magnitude~~presents much lower activities, with an average of 0.7 dpm l^{-1} (Fig. 6a-d). Activities of ^{224}Ra and ^{223}Ra are fairly uniform and low ~~with depth~~ in ADE-17 and ADE-1 ~~(although (~~ ~~^{224}Ra is~~ slightly higher in the epigenetic section~~), while~~), while significantly higher ~~activities~~ in the more saline ground ice of ADE-2 ~~samples~~ (epigenetic section~~) are significantly higher (~~; Figs. 6a- b and 7). ~~On the other hand,~~ ^{226}Ra and ~~is~~ ^{228}Ra ~~similar a bit~~also show higher activities in ~~higher in the epigenetic section~~ the epigenetic, compared with the syngenetic section, with no difference between the cores, and ~~in all three cores, showing no trend with depth, although~~with the ~~the highest activities in ADE-17~~ highest activities ~~were~~ observed at the top of the ~~epigenetic~~ section (6-10 m depth, Fig. 6c-d). ~~^{228}Ra activities are higher in the epigenetic section (Fig. 6d).~~

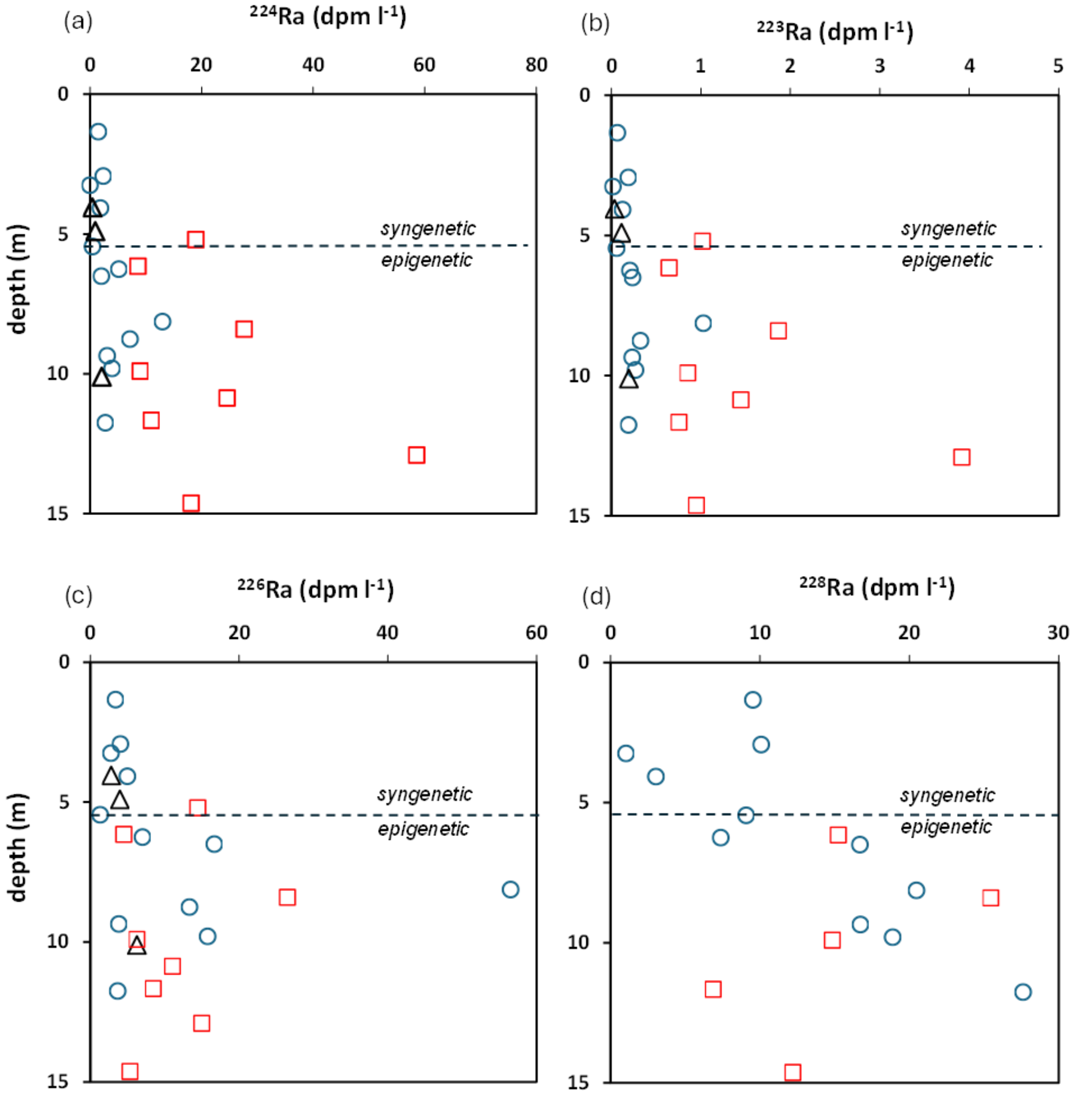

~~**Figure 6: Radium isotope activities in ground ice of the three ADE cores. The dashed line as in Figure 3**~~

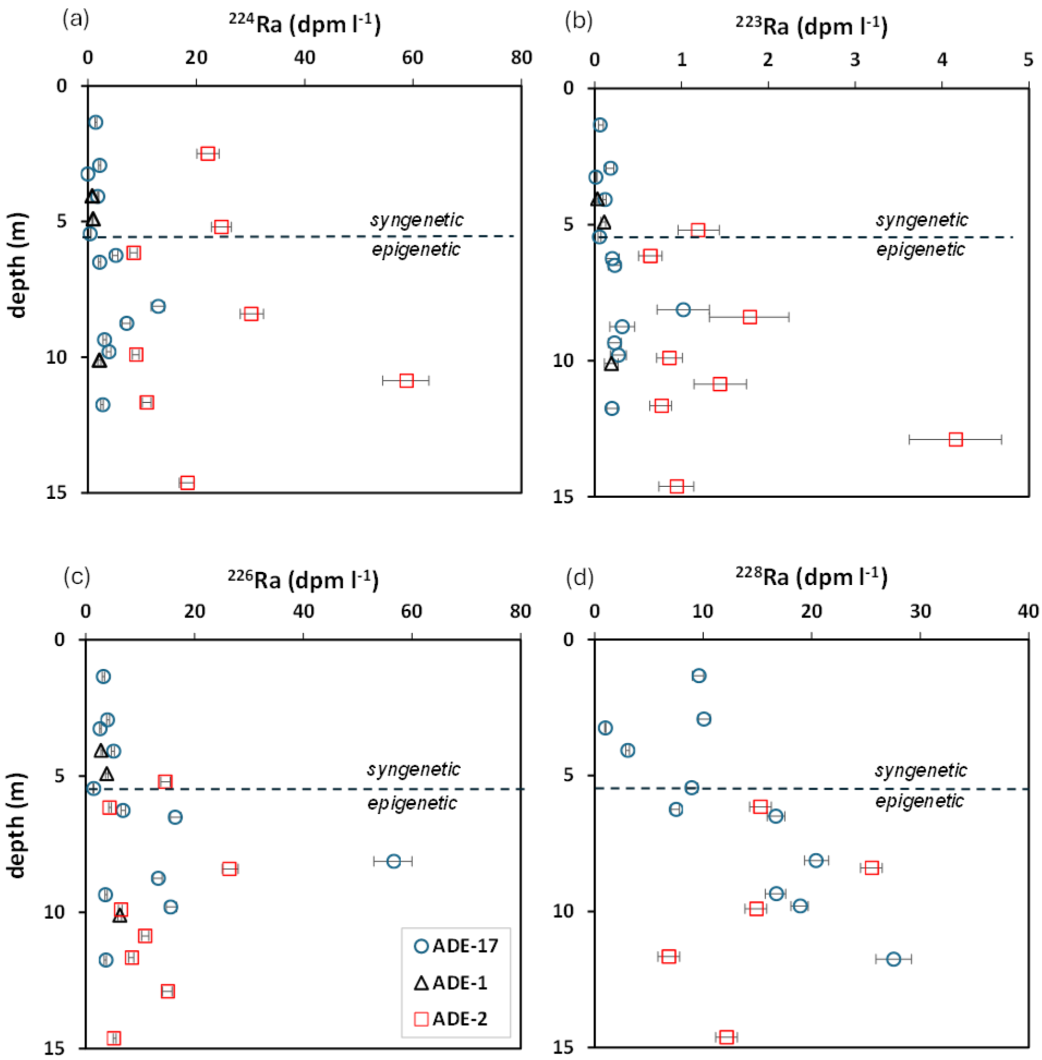

Figure 6: Radium isotope activities in ground ice of the three ADE cores. The dashed line as in Figure 3.

Ratios of the long to short-lived radium isotopes, (^{226}Ra/^{223}Ra)$_{AR}$, demonstrate a large range (4 to 72; Fig. 8a, with three outliers >100). Nevertheless, there are with marked differences between the cores. While in ADE-17 and ADE-1, (^{226}Ra/^{223}Ra)$_{AR}$ ratios both in syngenetic and the epigenetic section are close or higher than the secular equilibrium activity ratio (21.7, which is the natural ratio of parent nuclides ^{238}U/^{235}U, e.g., Kiro et al., 2015; Weinstein et al., 2021), ratios in ADE-2 (epigenetic section) are relatively low, ranging between 4-14 (Figs. 7c and 8a). Altogether there are marked differences between the cores.

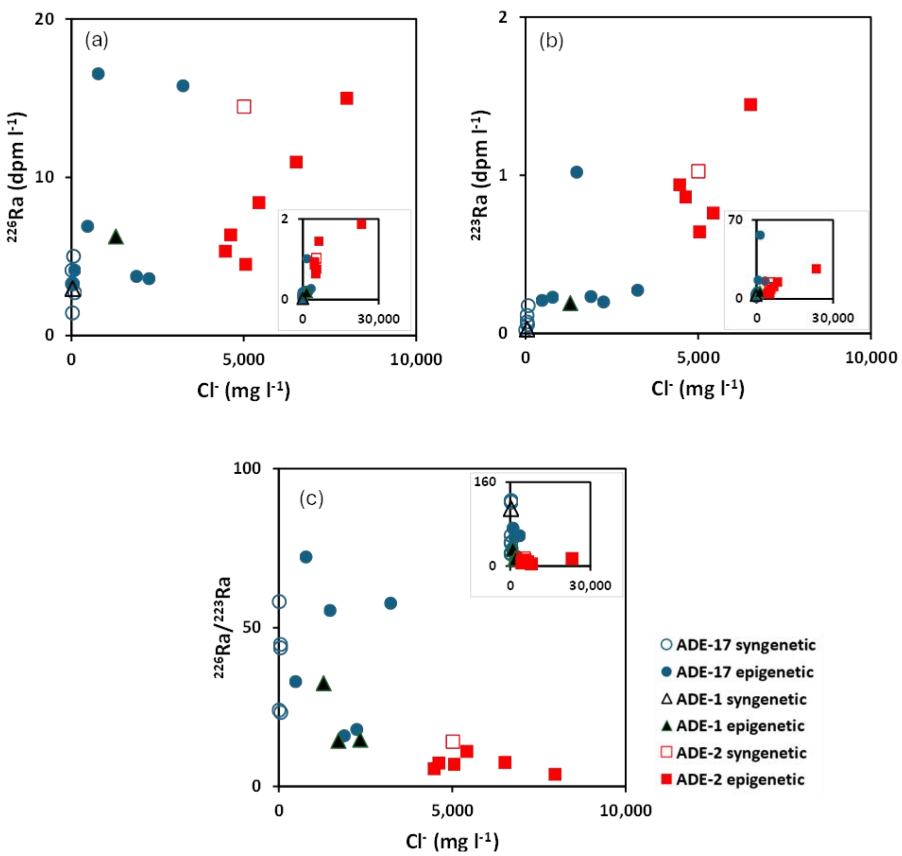

Figure 7: Radium isotope activities and ratios against chloride. (a) ^{223}Ra, (b) ^{226}Ra, (c) ^{226}Ra/^{223}Ra.

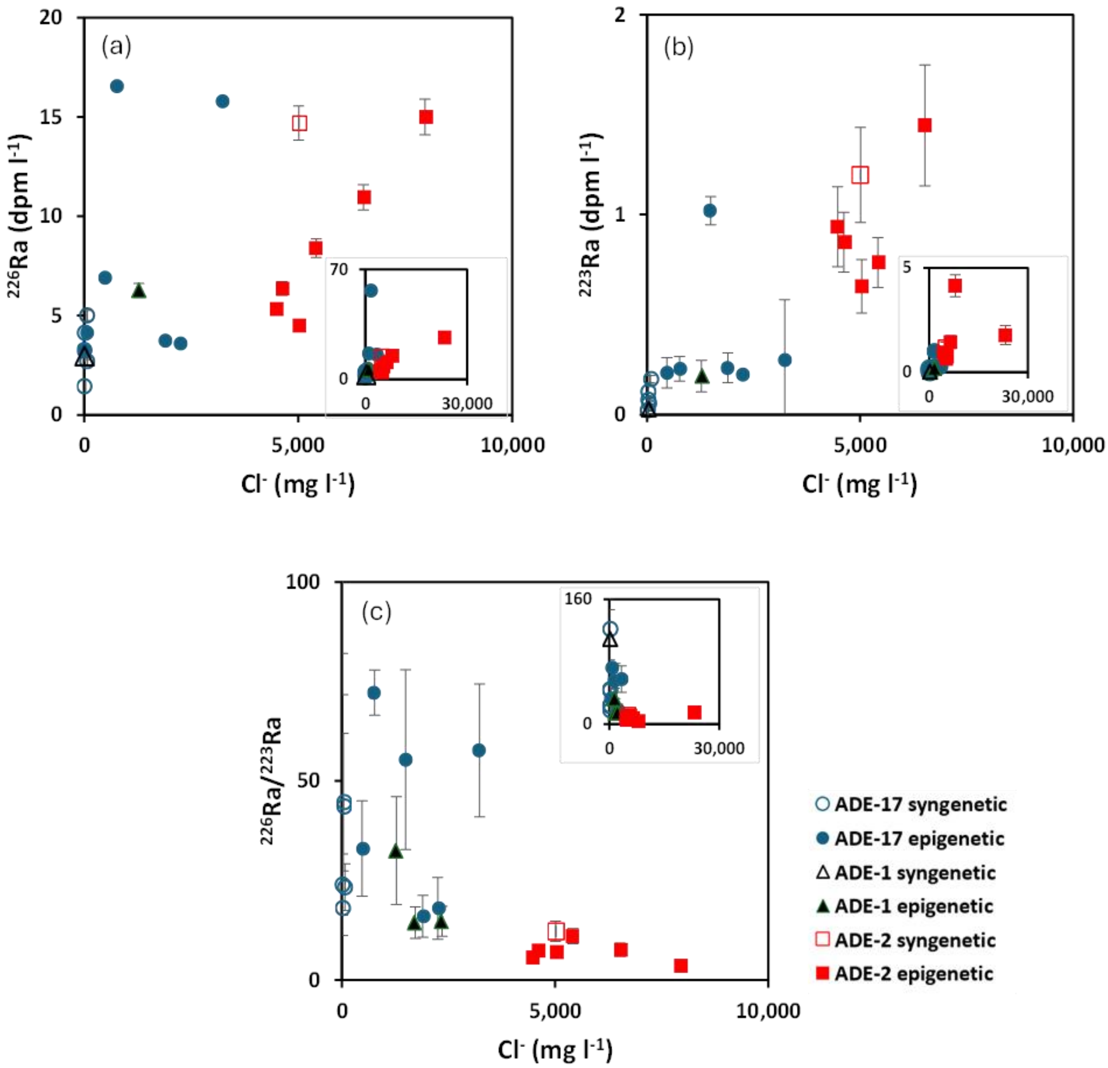

Figure 7: Radium isotope activities and ratios against chloride. (a) ~~^{223}Ra~~^{226}Ra, (b) ~~^{226}Ra~~^{223}Ra, (c) ^{226}Ra/^{223}Ra.

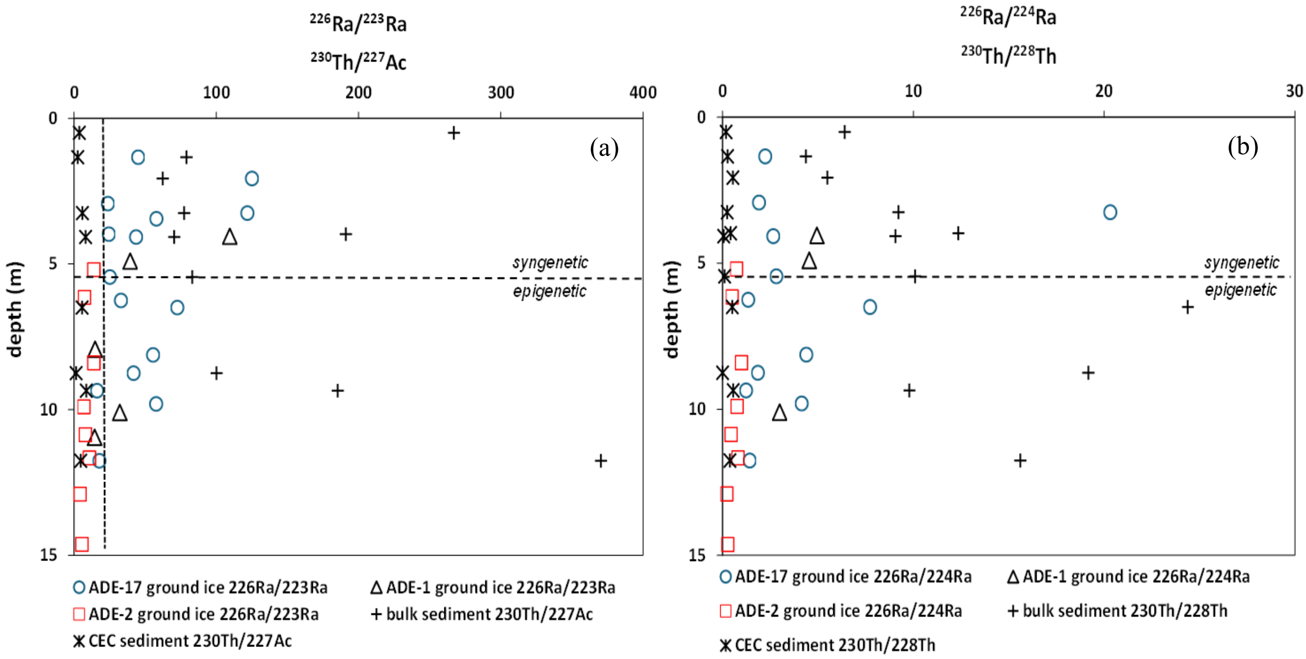

~~**Figure 8: Radium isotope activities in ground ice and their parent ratios in bulk soil grains and on grain surfaces (CEC, for Cation Exchange Capacity). (a) (^{226}Ra/^{223}Ra)$_{AR}$ and (^{230}Th/^{227}Ac)$_{AR}$; (b) (^{226}Ra/^{224}Ra)$_{AR}$ and (^{230}Th/^{228}Th)$_{AR}$. The vertical dotted line in (a) indicates the secular equilibrium ratios of (^{235}U/^{238}U), parents of ^{226}Ra and ^{223}Ra, respectively. The dashed line as in Figure 3**~~.

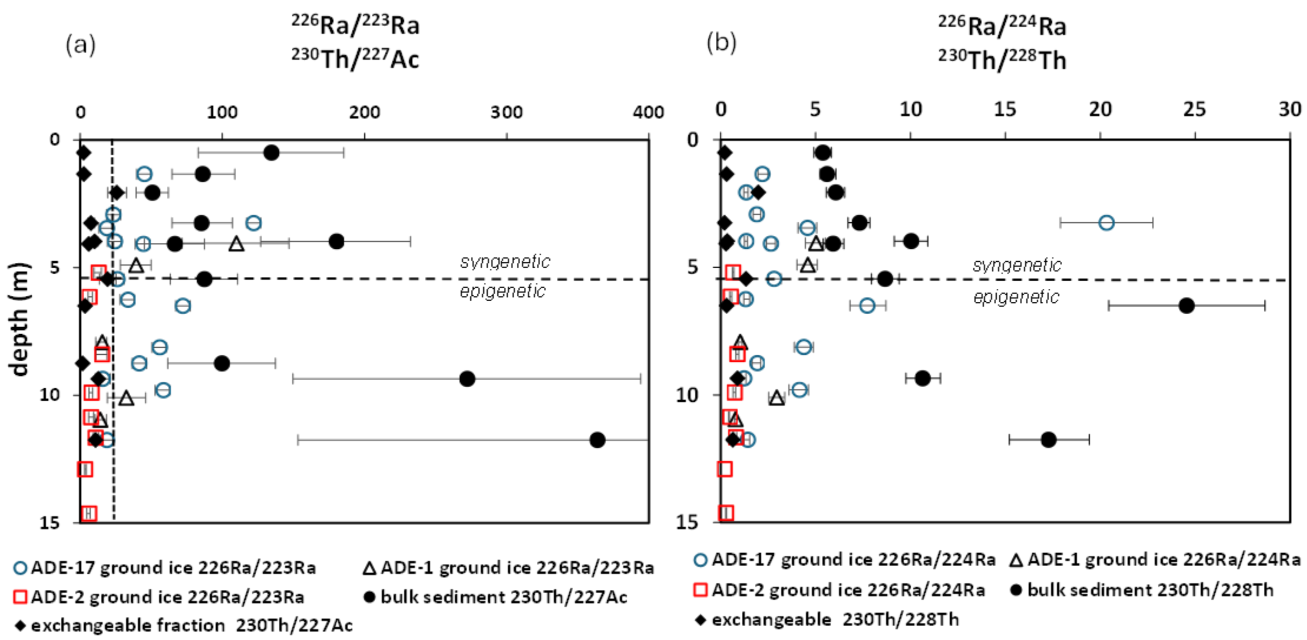

Figure 8: Radium isotope activities in ground ice and their parent ratios in bulk soil grains and on grain surfaces (exchangeable fraction~~CEC, for Cation Exchange Capacity~~). (a) (^{226}Ra/^{223}Ra)$_{AR}$ and (^{230}Th/^{227}Ac)$_{AR}$; (b) (^{226}Ra/^{224}Ra)$_{AR}$ and (^{230}Th/^{228}Th)$_{AR}$. The vertical dotted line in (a) indicates the ~~secular equilibrium~~natural ratio~~s~~ of (~~^{235}U~~^{238}U/~~^{238}U~~^{235}U), parents of ^{226}Ra and ^{223}Ra, respectively. The dashed line as in Figure 3.

$(^{226}Ra/^{224}Ra)_{AR}$ shows a similar pattern, where ratios in ground ice from cores ADE-17 and ADE-1 are higher than those in ADE-2 samples (>1and 0.3-1, respectively, Fig. 8b). The ratio of ^{226}Ra to the medium-lived (half-life of 5.75 years) ^{228}Ra is mostly ≤1, with no difference between the cores (Table C3C2), although some of the ADE-17 samples show ratios >>1. The daughter-parent ratio $(^{224}Ra/^{228}Ra)_{AR}$ in ADE-17 ranges between 0.13-0.68 (outlierof 1.0), while in ADE-2, ratios in the epigenetic part are mostly higher (0.55-1.58, Fig. 9).

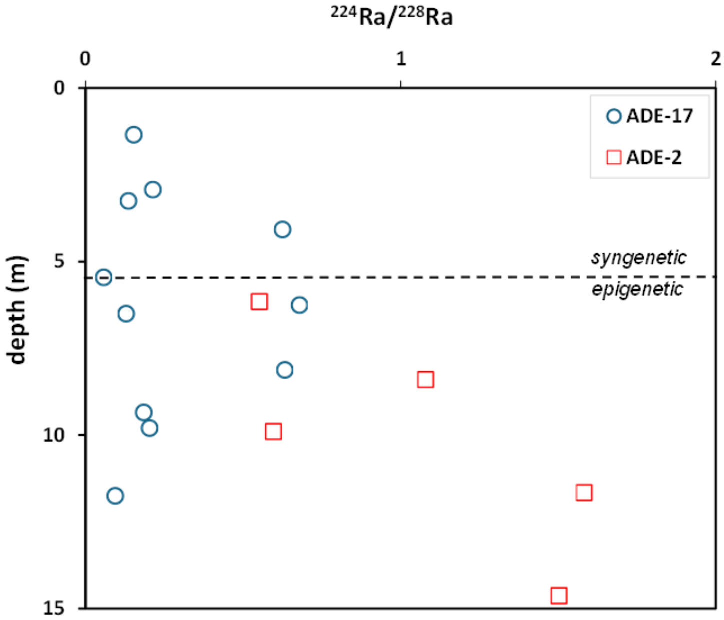

Figure 9: $(^{224}Ra/^{228}Ra)_{AR}$ in the ADE cores. The dashed line as in Figure 3.

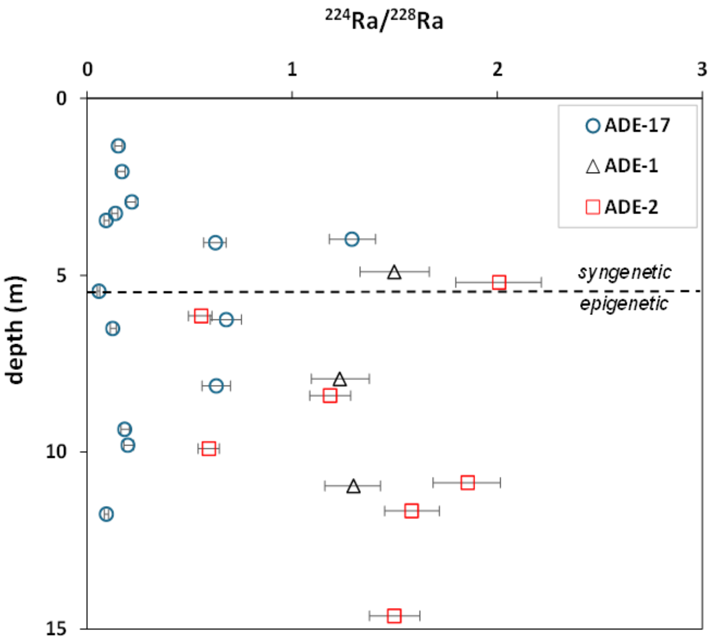

Figure 9: $(^{224}Ra/^{228}Ra)_{AR}$ in the ADE cores. The dashed line as in Figure 3.

4.3. Thorium isotopes and ^{227}Ac in permafrost soil

Thorium isotope activities in soil samples (bulk and exchangeable fraction CEC) from core ADE-17 are presented in Table C3. While ^{232}Th and ^{230}Th activities in bulk samples are two to three orders of magnitude higher than in the CEC exchangeable fraction (4.3-8.4 and 0.01-0.17 dpm g^{-1}, respectively), reflecting their main residence inside the grains (mineral lattice). On the other hand, ^{228}Th activities in the exchangeable fraction CEC are similar to those in the bulk (both are in the range of 0.1-1.2 dpm g^{-1}, Table C3 and Fig. 10), implying that most of the latter is adsorbed onto grain surfaces. Importantly, although being progeny of ^{232}Th, ^{228}Th activities are, on the average, twice the ^{232}Th activities in the exchangeable fraction. This is due to the fact that ^{228}Th is also produced from ^{228}Ra that recoiled via the decay of ^{232}Th close to grain rims.T his The above is also true for ^{227}Ac (Table C3), where exchangeable fraction CEC activities are close (though lower) to bulk activities. This is especially true for the epigenetic section, while in the syngenetic part, bulk sediment ^{228}Th is up to 12 times that in the exchangeable fraction CEC (i.e., grain surface ^{228}Th is not dominant, Fig. 10), although still lower from bulk/exchangeable CEC ratios of ^{232}Th and ^{230}Th (10's to 100's, Fig. 10).

(^{230}Th/^{232}Th)$_{AR}$ in the bulk sediment is quite uniform along the whole permafrost section, ranging between 0.7-1.0 (Table C3). ; nNote that these are activity ratios, while concentration ratios average 5x10^{-6}). Ratios in the exchangeable CEC fraction change from <1 in the syngenetic permafrost to >1 in the epigenetic section (5 – 12 m depth). (^{230}Th/^{227}Ac)$_{AR}$ in bulk sediment are significantly higher than the secular equilibrium activity ratio (21.7, Fig. 8a), while all exchangeable fraction CEC samples show lower than equilibrium activity ratios (2-12, Table C3, and Fig. 8a). This differenceThe latter is apparently due to the high concentration of ^{227}Ac on grain surfaces. Notably, daughter ratios, (^{226}Ra/^{223}Ra)$_{AR}$ in ground ice of ADE-2 is similar (slightly higher) to the (^{230}Th/^{227}Ac)$_{AR}$ in the exchangeable CEC fraction, while in ADE-17 ratios are much higher, 'mid-way', between CEC the exchangeable fraction and bulk sediment ratios (Fig. 8a). (^{230}Th/^{228}Th)$_{AR}$ shows a similar pattern, with exchangeable fraction CEC ratios being much lower than the bulk sediment ratios, and with the daughter (^{226}Ra/^{224}Ra)$_{AR}$ in the ground ice of ADE-2 being similar to the exchangeable fraction CEC parent ratios and those of ADE-17 and ADE-1 positioned mostly between exchangeable fraction CEC and the bulk sediment ratios (Fig. 8b).

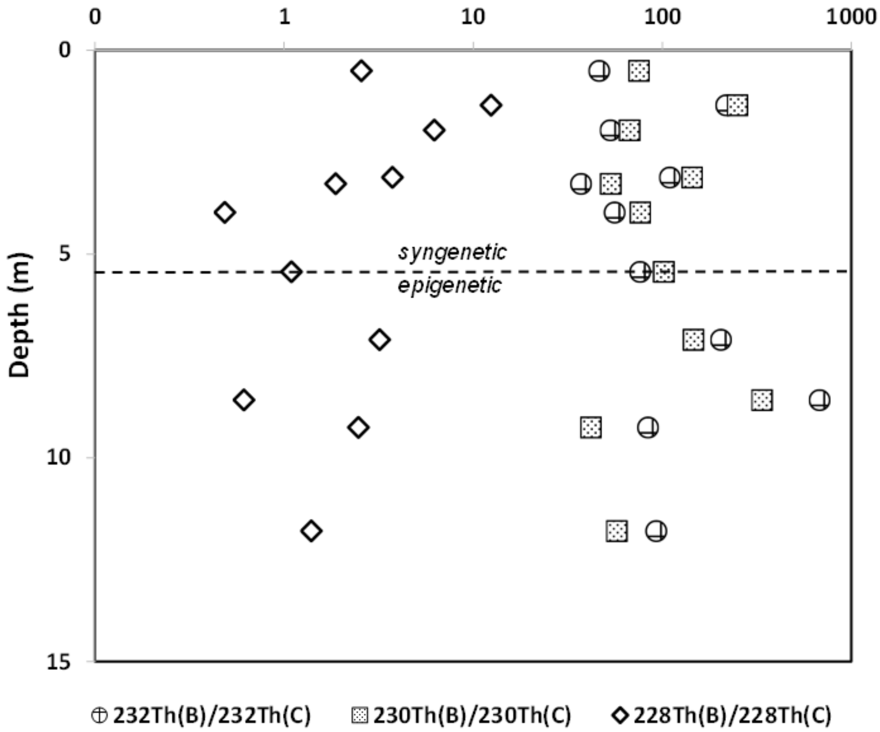

~~Figure 10: Bulk sediment/CEC (B/C) activity ratios of thorium isotopes in sediments from ADE-17. The dashed line as in Figure 3. Note the logarithmic scale.~~

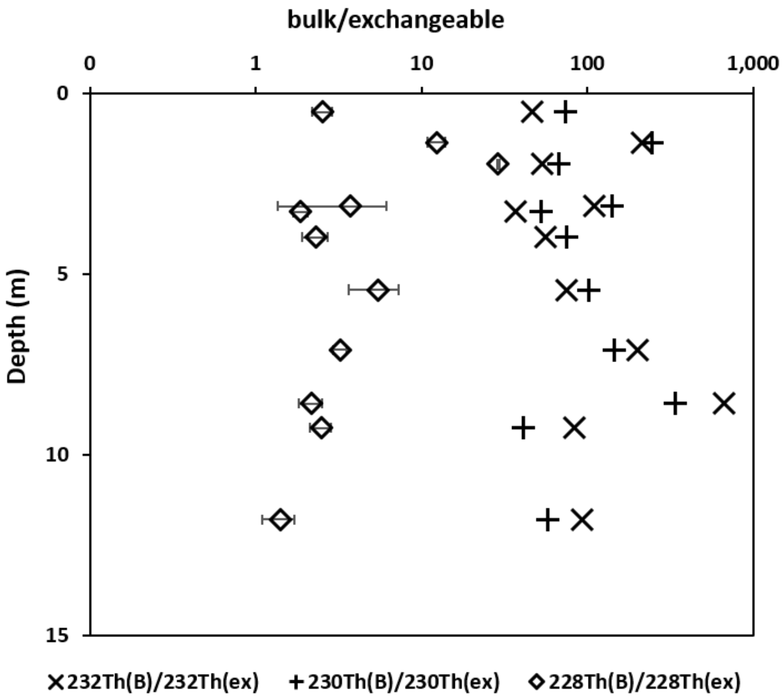

Figure 10: Bulk sediment/~~CEC~~ exchangeable (B/~~C~~ex) activity ratios of thorium isotopes in sediments from ADE-17. The dashed line as in Figure 3. Note the

5. Discussion

5.1. The heterogeneous nature of ground ice in Adventdalen

Our study site is located within the reach of the marine early Holocene transgression (Fig. 1, Gilbert et al., 2018), suggesting a-priori that the saline water observed in the permafrost epigenetic section is of an estuary-marine origin. Nevertheless, ground ice retrieved from the same depths in the three cores, located ≤30 m apart (Fig. 1), differ markedly in their salinity and chemical composition, as well as in their radium isotope ratios (Figs. 3-8). The salinity of ground ice from borehole ADE-2 is relatively high, with up to more than seawater salinity and no distinct pattern with depth (Fig. 3). In ADE-17, salinity does not exceed 20% that of seawater, and it increases with depth in the epigenetic section. Finally, in ADE-1, salinity is less than 6-7% that of seawater, and no distinct pattern is observed. The difference between the cores is not just about the extent of dilution with fresh water/ground ice, but also about the contribution of water:rock interaction, as demonstrated by the ionic ratios. While in ADE-2, ionic ratios are relatively similar to seawater (Figs. 4 and 5; although Na/Cl of 1 could indicate halite dissolution in some of the samples and high SO_4/Cl in two of the samples could be due to sulfide oxidation, possibly related to the coal layers, common in the nearby slopes), ground ice from ADE-17 and ADE-1 shows Na/Cl and SO_4/Cl significantly higher than in seawater (~~although still lower than in the syngenetic part;~~ Figs. 4 and 5a-b). The similar to seawater chemistry in ADE-2 ground ice favors a marine source for its saline component. ~~The~~ On the other hand, the >1 Na/Cl in ADE-17 and ADE-1 (compared with 0.86 in seawater) suggests that, although it probably also contains a seawater component, porewater in these two cores went through significant water-rock interaction (WRI, e.g., dissolution or ion exchange). Accordingly, this water is the result of both mixing between fresh, meteoric water and Early Holocene seawater and of WRI. It should be noted that seawater freezing and saline fluid expulsion could not be a significant player here, since in this case fractionation would result in Na/Cl ratios lower than that of seawater (e.g., Herut et al., 1990), which is ~~not the case in any of the samples~~hardly observed (see fresh-seawater mixing line in Fig. 4a).

The observation of a high salinity profile in ADE-2 all the way to the top of the epigenetic, marine section could be the result of an immediate freezing following exposure to the atmosphere (e.g., Rotem et al., 2023), which limited mixing with fresh water, as well as reduced the effect of WRI. However, the fact that this profile is very different from the nearby boreholes, including its salinity, composition and pattern with depth, favors a later introduction of saline water into the permafrost pore space at this location, which could occur either via intrusion or by intra-permafrost segregation processes (e.g., Ahonen, 2001; French, 2007; Iwahana et al., 2021). Late Holocene intrusion of a saline fluid is firmly supported by the fact that the high salinity in ADE-2 continues into the syngenetic section (Table 1 and Fig. 3), which has been deposited during 4-2 ka (Gilbert et al., 2018). ~~Our~~ This will be further discussed in light of the radium ~~results, support this post-permafrost formation scenario~~and thorium isotope data, as follows.

5.2. Radionuclides insights into ground ice timing

The differences in chemistry between the cores are accompanied by differences in the Ra isotope ratios, where long to short-lived isotope activity ratios ($^{226}Ra/^{224}Ra$ and $^{226}Ra/^{223}Ra$) are significantly lower in the ground ice of ADE-2, compared with that in ADE-17 and ADE-1 (Figs. 8a-b). In particular, while $(^{226}Ra/^{223}Ra)_{AR}$ in ADE-17 and ADE-1 are ≥20, in ADE-2 these ratios are ≤14 (Fig. 8a). The low ratios in ADE-2 are apparently because activities of the short-lived isotopes are significantly higher than in the two other cores (Fig. 6b), while ^{226}Ra activities are quite similar (Fig. 6a). However, the significantly higher salinity in ADE-2 should result in higher activities of all radium isotopes in this core due to the reduced adsorption (e.g., Kraemer and Reid, 1984; Gonneea et al., 2008; Kiro et al., 2012; Vinson et al., 2013), and assuming a non-complete frozen nature of the permafrost (e.g., Gilbert et al., 2019; Keating et al., 2018; Weinstein et al., 2019). ~~However, t~~The observation that this is the case only with the short-lived isotopes, while not with the long-lived ^{226}Ra, raises the possibility of a timing control on the radium isotopes of ground ice in this core (e.g., Weinstein et al., 2019, 2021), namely that the relatively low ^{226}Ra (compared with 223Ra) is ~~due to~~the result of a short residence time of the ADE-2 ground ice. Time constraints will be further discussed below.

Another important observation is that in ADE-2, both $(^{226}Ra/^{223}Ra)_{AR}$ and $(^{226}Ra/^{224}Ra)_{AR}$ activity ratios in ground ice are similar to (i.e., close to equilibrium with) their parent nuclide activity ratios ($^{230}Th/^{227}Ac$ and $^{230}Th/^{228}Th$, respectively) in the exchangeable ~~CEC sediment~~ fraction (i.e., surface of grains). On the other hand, in ADE-17 radium ratios are consistently higher and are closer to parent ratios in the bulk sediment (Figs. 8a-b). We note that while Th and Ac isotope activities were measured only in the ADE-17 sediment, the very close proximity of the cores (within 30 m) and the relatively uniform Th isotope ratios in the exchangeable fraction along the sediment profile (~~at least regarding the CEC,~~ Table C3) suggest that the measured sediment nuclide ratios, in particular the differences between ratios in bulk and the exchangeable fractions, should not be very different between the ADE core locations.

In fact, ^{226}Ra activities in ground ice (1-60 dpm l^{-1}) of all three cores are significantly lower than the ^{230}Th activities in the exchangeable fraction ~~CEC~~ (0.02-0.17 dpm g^{-1}, Table C3), which considering a dry solid density of 2.5 g/cc ~~and~~, a relatively high porosity of 50% (100% ice content, Table C1) and recoil release fraction of 50%, is equivalent to ~~50-425~~25-200 dpm l^{-1} (Fig. 11; a more conservative porosity of 25% ~~will~~ would ~~triplicate~~ triple these activities). The much lower ~~than calculated~~ ^{226}Ra activities in the ground ice are probably the result of most of recoiled radium being kept on grain surfaces (Fleischer and Raabe, 1978; Suksi and Rasilainen, 1996)~~,~~, either physically-attached or adsorbed, if liquid water is present~~or concentrated in liquid films attached to the grains~~. Notably, ~~sample~~ ground-ice of DR-AD-125, which is characterized by an exceptionally high salinity (Cl^- higher than in seawater, Fig. 4, Table C1), showed unusually high radium activities of all isotopes (Table C2), probably due to lower radium adsorption onto grains.

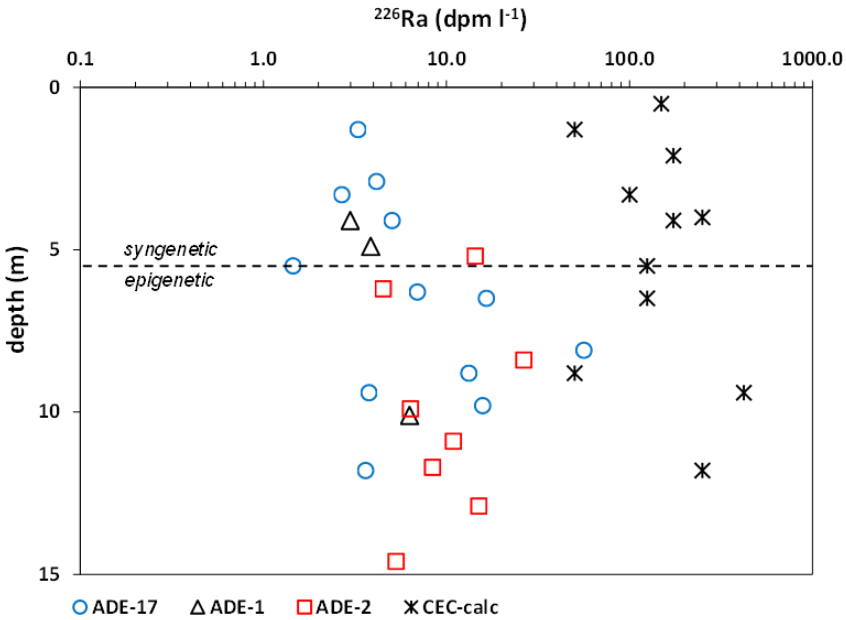

~~**Figure 11: ^{226}Ra (dpm l^{-1}) in ground ice of the three ADE cores and its calculated activities on CEC (CEC-calc) fraction. Note the logarithmic axis. The dashed line as in Figure 3.**~~

5.2.1 Ground ice residence times

The similarity between (^{226}Ra/^{sl}Ra)$_{AR}$ (sl = 'short-lived') ratios in ADE-2 and the ~~^{230}Th/~~parent nuclide activity ratios in the exchangeable ~~CEC~~ fraction (Fig~~s~~. ~~7 and~~ 8) suggests that pore space radium isotopes are in equilibrium with parent nuclides on grain surfaces. Equilibrium activity ratios of radium isotopes are supposed to be achieved within 5-6 half-lives of the longer-lived isotope (i.e., ^{226}Ra, with a half-life of 1600 years), or shorter if adsorption is involved (Kiro et al., 2013; Weinstein et al., 2021). The concentration of a certain Ra isotope in ~~groundwater~~ pore space (water or ground ice) at time t is described by Equation (1), assuming steady production and negligible dissolution and diffusion (e.g., Kiro et al., 201~~5~~3; Weinstein et al., 2021), as is probably the case in the ground ice.

$$~~C~~ A = \frac{P}{\lambda(K+1)}\left(1 - exp^{-\lambda(K+1)t}\right) + ~~C_0~~ A_0 exp^{-\lambda(K+1)t} \quad (1)$$

~~C~~ A is the activity [dpm l^{-1}] of the isotope, ~~C_0~~ A_0 is the initial activity [dpm l^{-1}] (when the fluid/ice was emplaced in pore space), P is the production by recoil from the sediment [dpm l^{-1} yr^{-1}], λ is the decay constant of the isotope [yr^{-1}] ~~and~~, K (=R+1; Krishnaswami et al., 1982) is ~~a~~ the unitless adsorption coefficient and t is the time since water (or ice) emplacement in the pore space [yr]. The actual activities of ^{226}Ra in our samples are controlled by adsorption, as well as by the efficiency of the (thawed) ground ice extraction. Accordingly, we prefer to normalize ^{226}Ra to ^{223}Ra activities. The short-lived isotopes ^{224}Ra and ^{223}Ra reach steady state activities within weeks, which for the discussed time scales practically means a uniform activity. ~~Accordingly, we will make use of the average isotope activity in ADE-2 e.g. 1.4 dpm l^{-1} for ^{223}Ra (Table C2).~~ Therefore, ratios of long to short-lived isotopes solely depend on the initial ratio and on the buildup of ^{226}Ra activities.

In Fig. 1~~2~~1, we show the buildup of (^{226}Ra/^{223}Ra)$_{AR}$ in the ground ice with time. For ^{223}Ra, we make use of the average isotope activity in ADE-2, e.g., 1.4 dpm l^{-1} (Table C2; stdev is 1.1 dpm l^{-1}, which is mainly due to one sample of 3.9 dpm l^{-1}).

While C_0 of ^{226}Ra is not well-constrained for the shallow (syngenetic) layers, we ~~may~~ assume that fluid in the the deeper, epigenetic layers had initial activities similar to that of typical shelf seawater (e.g., 0.1 dpm l^{-1}, Moore, 1996). This is a minimum value, because fluid could reside in pore space much before ground ice formation, but will not change the pattern of buildup to steady-state ratios, as discussed below. ~~In Fig. 12, we show the buildup of ($^{226}Ra/^{223}Ra)_{AR}$ in the ground ice with time.~~ Assuming that ~~no adsorption (K=0 for a completely frozen pore space)~~ground ice radium in ADE-2 is produced only from the exchangeable fraction,~~,~~ the time that will take ($^{226}Ra/^{223}Ra)_{AR}$ ~~will~~ to reach exchangeable (~~CEC~~ $^{230}Th/^{227}Ac)_{AR}$ ~~activity ratios~~ is dependent on the adsorption.~~(secular equilibrium) within several thousands of years . We note that even if initial ^{226}Ra activities is an order of magnitude higher, the time to reach equilibrium values would be similar (see Fig. 12). Times could shorten significantly if liquid is present in the pore space, as is sometimes the case in the studied area~~With K=0 (i.e. R-1), ~~-~~this will take several thousand years. On the other hand, if some liquid is present in pore space (e.g., Keating et al., 2018; Weinstein et al., 2019), ~~thus allowing~~this will result in adsorption joining the process~~to take place~~, and calculated residence ~~. For instance~~times will significantly shorten~~, if~~. For instance, with K=10 , as is the case for seawater salinities, (e.g., Weinstein et al., 2021; Garcia-Orellana et al., 2021; Diego-Feliu et al., 2021), time to reach equilibrium will be on the order of 100's years, and with K=100 times will reduce to 10's years. ~~However,~~ We note that the cryotic conditions and the more common observation of a frozen pore space do not favor too much adsorption. Accordingly, while the Th- Ra secular equilibrium cannot be quantitatively used for residence time determination, it still indicates that the ground ice in ADE-2 has not been recently formed, and that it is ~~probably~~ at least ~~100's years~~decades old. On the other hand, importantly, the relatively low ($^{226}Ra/^{223}Ra)_{AR}$ in ADE-2 indicates that there is no significant contribution from inside the grains, since judging by the high ($^{230}Th/^{227}Ac)_{AR}$ of the bulk sediment, this should result in higher ($^{226}Ra/^{223}Ra)_{AR}$. ~~The~~ Below, we use this observation and the circumstantial evidence of the high salinity in the syngenetic section of ADE-2 to infer about the mechanism that is responsible for the higher ($^{226}Ra/^{223}Ra)_{AR}$ in the other cores.~~upper limit on the residence time in ADE-2 should be achieved by circumstantial observations, as follows.~~

As noted, and unlike ADE-2, ($^{226}Ra/^{sl}Ra)_{AR}$ in ground ice of ADE-17 (and ADE-1) are significantly higher than the ~~CEC~~ exchangeable fraction parent nuclide ratios (e.g., ($^{226}Ra/^{223}Ra)_{AR}$ is mostly 20 - 70), being much closer to (although not in equilibrium with) bulk sediment parent $^{230}Th/^{227}Ac$ ratios (Fig. 8a). This suggests that on top of contribution from the ~~CEC~~ exchangeable fraction, there was enough time in ADE-17 for some ^{226}Ra to arrive from a different source, e.g., from inside the grains. While contribution from the grains could be accomplished by direct recoil from grain rims, there is no reason for this not to happen within the same time scale as that of the exchangeable fraction, which is not the case in ADE-2. Alternatively, we suggest that this contribution is via ^{226}Ra ~~diffuse~~ diffusion out of the mineral grains, which is time-dependent (see 5.2.2). On the other hand, this is not relevant for ^{223}Ra, ~~with~~ which with a half-life of 11 days, ~~is not relevant for~~cannot benefit by diffusion from inside the grains, ~~and does not reach the pore space, therefore~~hence the high ($^{226}Ra/^{223}Ra)_{AR}$ in ADE-17.

Unfortunately, we have no good control on diffusion rates under cryo~~e~~tic conditions (see discussion in section 5.2.2), but the maximum time allowed for ground ice formation in the study site could be ~~easily~~ circumstantially constrained. Valley-fill marine sediments at the ADE site are of Early Holocene age (≤10,500 years, e.g., Lønne and Nemec, 2004), and permafrost formation (i.e., freezing) occurred no earlier than 9.5 ka, after being exposed to the atmosphere due to the elastic rebound (e.g., Gilbert et al., 2018; Rotem et al., 2023). This means that no ground ice is ~~no~~ older than Early Holocene, and that 9-10 kyr has been enough time for a significant diffusion of ^{226}Ra ~~from inside the~~out

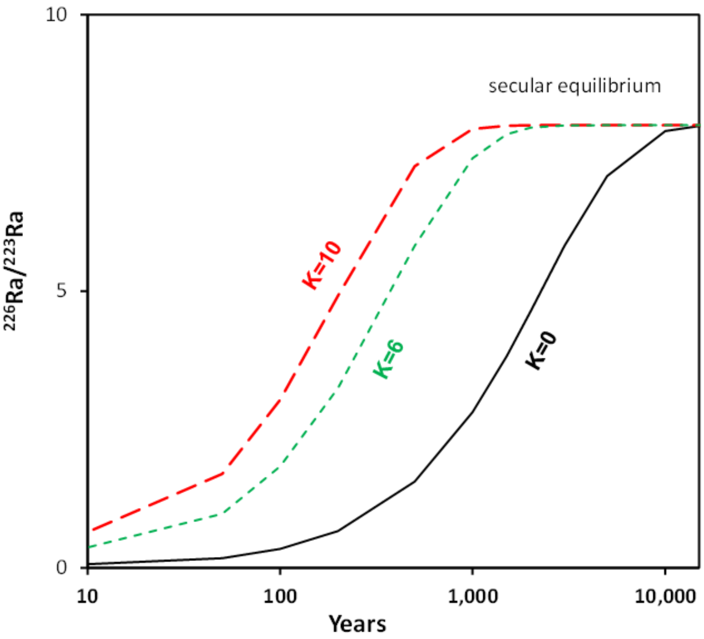

~~**Figure 12: Simulations of the buildup of (^{226}Ra/^{223}Ra)$_{AR}$ in permafrost pore space with different adsorption coefficients (K=0 means no adsorption). See text for further explanations.**~~

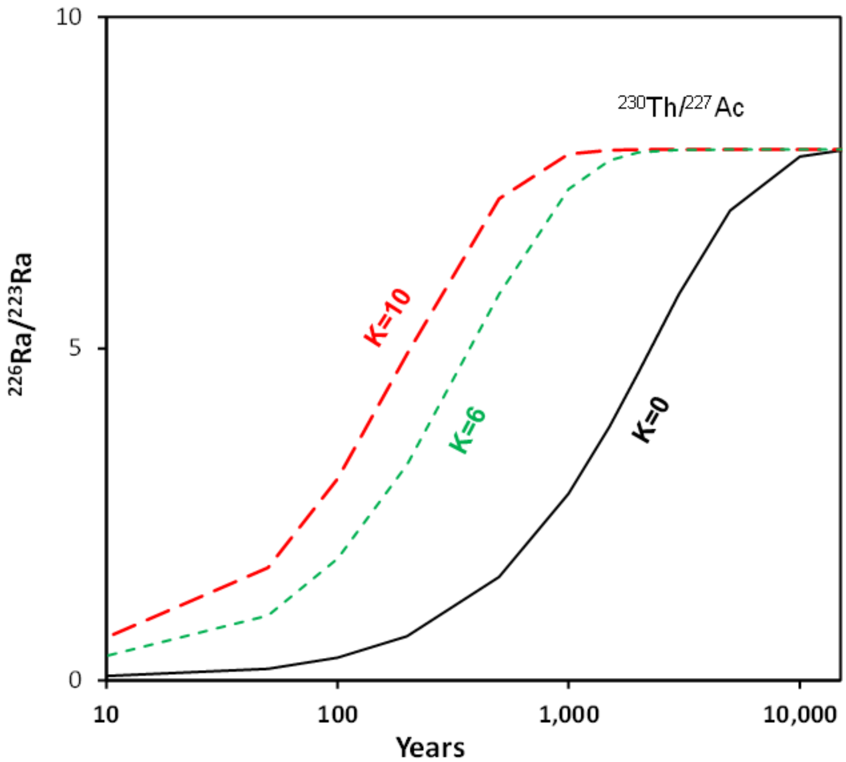

Figure ~~12~~11: Simulations of the buildup of (^{226}Ra/^{223}Ra)$_{AR}$ in permafrost pore space with different adsorption coefficients (K=0 means no adsorption). See text for further explanations.

of grains ~~to occur~~ in ADE-17. Moreover, high (^{226}Ra/^{sl}Ra)$_{AR}$ are also found in the syngenetic (shallow) part of the permafrost profile (Fig. 7a), which has been deposited between 4-2 ka (Gilbert et al., 2018). This implies that even 4-2 thousand years are enough for a significant diffusion of ^{226}Ra out of the grains (probably, from outer portions). ~~As a matter of fact, only Only a small fraction of the produced ^{226}Ra has to diffuse out of the grains in order to produce the high (^{226}Ra/^{sl}Ra)$_{AR}$. With a bulk ^{230}Th of 4-8 dpm/g (Table C3), a dry density of 2.5 g/cc, porosity of 25-50% (i.e., 50-100% ice content, Table C1) and 50% emanation (release to pore space), ^{226}Ra in ground ice should be as high as 20,000-100,000 dpm/l, which is 3-4 orders higher than that observed in the ground ice (Table C2).~~

~~Based on the observations in ADE-17 and its time scales,~~ This means that the consistently lower (^{226}Ra/^{sl}Ra)$_{AR}$ in the epigenetic ground ice of core ADE-2 constrains its residence time (probably, the reset of the residence time clock) to <<2,000 years (Fig. ~~13~~12). This is supported by the observation of the high salinity also in the syngenetic part of the ADE-2 core (e.g., Table C1 and Figure 3), which suggests that the salinization post-dated the deposition of the shallow sediments, i.e. younger than 2,000 years. The meaning of this short residence time is discussed in section 5.3. We note that the mentioned timing is only if one assumes a single event of ground ice formation or residence time reset. Alternatively, this could be a continuous process, which could start earlier than 2000 years but its main impact would have to be relatively recent, in order to allow salinization of the syngenetic, shallow permafrost, as well as to keep the ^{226}Ra relatively low. ~~We note that the mentioned timing is only if one assumes a single event of ground ice formation or residence time reset.~~

~~Alternatively, this could be a continuous process, which could start significantly earlier than 2000 years but its main impact would have to be relatively recent, in order to keep the ^{226}Ra relatively low.~~

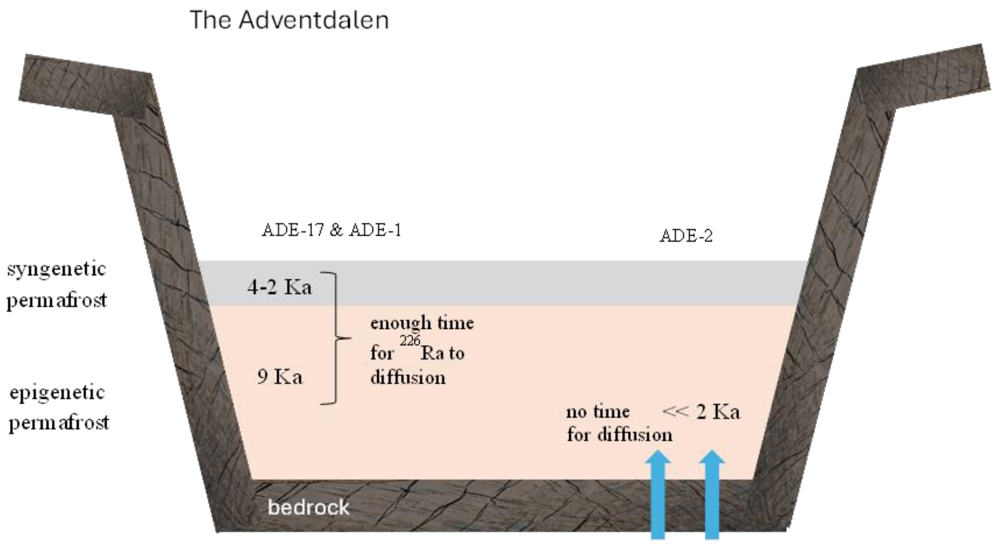

Figure ~~13~~12. Conceptual model of the heterogeneous nature of ground ice in the Adventdalen study site.

5.2.2 Diffusion from grains in the permafrost

Ra~~m~~ma and Moore (1984), showed experimentally that radon can diffuse out from sand grains within days, which was attributed to diffusion via nanopores. On the other hand, they argued that other, non-gaseous nuclides of the U-Th chains could not make it to the intergranular space, owing to adsorption in the nanopores. We believe that while radium diffusion could indeed be negligible in the short-term (days), it is not necessarily the case for the long term, i.e., 100's-1000's years. ~~Moreover, adsorption is orders of magnitude lower in saline water and hardly exists when pore space is frozen. Since~~while diffusion should be much slower and adsorption, higher under the low permafrost temperatures. ~~we deal with either completely or~~the high salinity and the probable frozen nature of the nano-pores could reduce ~~partially frozen saline ground ice, we believe that~~ adsorption ~~is less intense and that radium~~ allow diffusion from inside the grains ~~could be significant~~ especially, when thousands of years are considered. We also note that the ~~, in particular in~~ grain size discussed in this case is much smaller (silt and clay) than in the mentioned experiments (sand).

To the best of our knowledge, there is no data for low-T diffusion in solids, and there is hardly any data for sub-zero diffusion. Nevertheless, extrapolation from higher temperature data (e.g., for Ca) predicts D's (diffusion coefficients) in solids on the order of $<<10^{-24}$ m^2 sec^{-1} (e.g., Brady and Cherniak, 2010; Cherniak, 2010), which does not take into account the nanopore pathway. On the other hand, there is some data for diffusion of molecules (no single cations) in ice under a much lower than permafrost temperature (i.e., 100-140 ^{o}K), which is about 10^{-16} m^{2}cm^{-1} (e.g., Ghesquière et al., 2015). The effective diffusion coefficient in the permafrost soil grains should be dependent on the concentration of nano-pores, the cryotic condition of the fluid in the nano-pores, ~~and~~ porosity and liquid (if any) salinity. We suggest that main diffusion from inside the grains occurs through either completely or mostly frozen nano-pores. In Fig. ~~14~~13, we arbitrarily used effective diffusion coefficients of 10^{-23}-10^{-24} m^2 sec$^-$

[1] and distances relevant to clay minerals (0.5-2 µm) just in order to show that there could be a significant difference (up to one order of magnitude) in ^{226}Ra activities between Early and Late Holocene ground ice. Simulations were performed using the following equation: $Ra_p/Ra_g = erfc\{\frac{x}{2*\sqrt{De*\frac{t}{p*R}}}\}$, where Ra_p/Ra_g = activity in pore space relative to that in the grain, x=effective distance [m], De=effective diffusion coefficient [$m^2\ sec^{-1}$], t=time [sec], p=porosity [unitless], R=retardation factor [=K+1, unitless, Krishnaswami et al., 1982]. R was assumed 10 for saline water (e.g., Diego-Feliu et al., 2021). Note that the retardation is practically relevant only for liquidized nano-pores.~~,~~ We stress that the diffusion coefficients used for this figure are not based on any empirical data, and they were used only to show that diffusion could affect the long-lived ^{226}Ra. Slower diffusion rates (~~lowe~~ lower D's) or higher retardation values (e.g., Kumar et al. 2020) could still be effective with smaller diffusion distances (i.e., from outer part of the grain ~~rims~~, <<1µm). Fig. ~~14~~ 13 also shows that diffusion is strongly dependent on porosity. Another factor that affects diffusion is the retardation (i.e., adsorption), which is highly dependent on the existence of liquid, as well as on its salinity, redox, and pH conditions. In general, the higher the R, the lower the effective diffusion is. In Fig. ~~14~~13, we used R=10, which is for nanonpores filled with saline water (e.g., Weinstein et al., 2021; Garcia-Orellana et al., 2021). However, with nanopores being mostly or completely frozen, considering the cryotic conditions and the very low water:rock ratios inside the grains, the effect of adsorption is minimized, therefore R should be low even with fresh water.

To summarize this part, while we do not have low-T diffusion data, and while the effective diffusion is highly dependent on sediment texture and cryotic conditions, we do suggest that ~~pore space~~ground ice ^{226}Ra~~, thereby~~ and $(^{226}Ra/^{223}Ra)_{AR}$~~, is~~ are highly dependent on diffusion from grains, probably through froz~~n~~en nano-pores, reflecting on ground ice residence time.

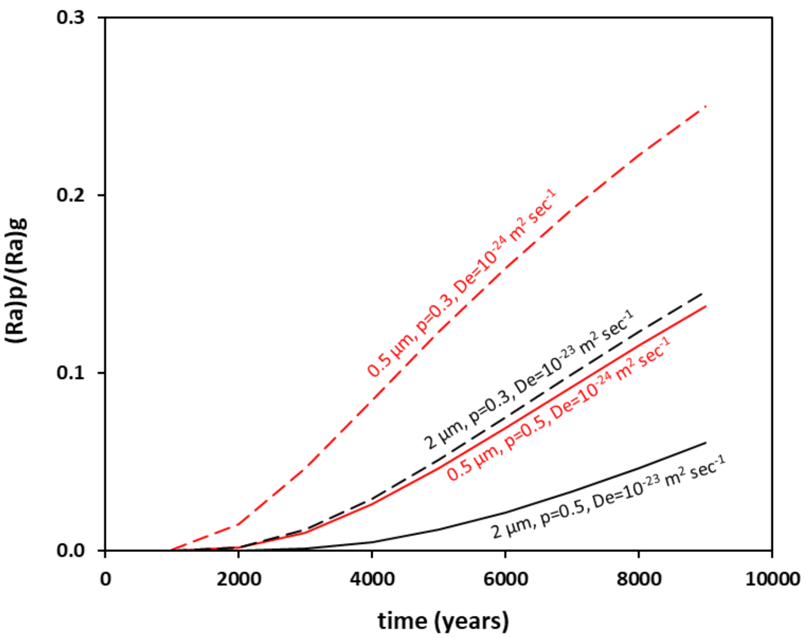

Figure ~~14~~13: Simulations of diffusion from sediment clay grains into the pore space. (Ra)p/(Ra)g = Ra activity in pore space normalized to that in grain. See text for the diffusion coefficients used. Solid and dashed lines are for high and low porosity (0.5 and 0.3, respectively). See text for explanation about the simulations.

5.3. Sources of ground ice and permafrost dynamics

The co-existence of pore fluids (ground ice) with different chemistry and supposedly distinct history (residence time) at the same site and depth (from the surface), and the comprehension that ~~the~~ ground ice formation (or re-generation) along the profile of one of the cores (ADE-2) is relatively young, calls for dynamic visualization of the permafrost at Adventdalen. Rotem et al.~~,~~ (2023) suggested that the saline water (and the frozen fresh-saline water interface) found at the top of the epigenetic section in ADE-17, at >10 m.a.s.l, has been preserved due to the immediate formation of permafrost following seawater regression from this site, ca. 9 ka. It is also apparent that some of the water went through water:rock interaction while in the sediment, probably prior to freezing (e.g., high Na/Cl and SO_4/Cl, Fig. 5), possibly when still covered with seawater.

Accordingly, the similar to seawater composition of the ground ice at ADE-2 and its implied short (<2000 yrs) residence time, as suggested by the $(^{226}Ra/^{sl}Ra)_{AR}$, which is supported by salinization intruding the young, syngenetic section, is quite enigmatic. A direct active connection to the nearby fjord, the Adventfjorden (Fig. 1) via sub-permafrost groundwater flow (i.e., seawater circulation) is unlikely because of the distance from the fjord (~10 km) and the depth it should gain following a Ghyben-Herzberg approximation (i.e., assuming a hydrostatic head close to the surface elevation of 23 m.a.s.l. and common seawater salinity, then the fresh-saline water interface should be at ca. 800-900 m depth; lower fjord water salinity should result in even deeper interface). Moreover, considering the basement geology (shales underlain by sandstones, e.g., Ogata et al., 2014) and the low hydraulic gradients involved (ca. 2‰, assuming it is parallel to the topographic gradient), the flow rate should not be much more than 1 m y^{-1} (e.g., Hornum et al., 2020), which would result in residence times of several thousand years at the study site, in discordance with the implied young age. Thus, it seems that the low $(^{226}Ra/^{sl}Ra)_{AR}$ at ADE-2 is the result of a Ra clock reset ('apparent' residence time) rather than due to actual residence time in the aquifer.

The buildup of radium isotope activity in the pore space, whether hosting water or ground ice, depends on several factors, including (1) the mineralogy of aquifer solids, (2) grain size and (3) pore space:solid ratio. The migration of water from Th-poor to a Th-rich lithology, as well as from high water:rock to low water:rock ratio environment, should result in an increased supply of radium, therefore possibly in the reset (or a partial reset) of the Ra isotope-ratio clock. Impact on radium release and resultant reset will be even stronger, if the intruding water is more saline than the older one (assuming a non-completely frozen environment), therefore reducing the adsorption effect. Accordingly, it is suggested that the ground ice in ADE-2 recently experienced a local intrusion of saline water, which previously resided in a low-Th or a high water:rock ratio aquifer. Such an aquifer could be the Early Cretaceous sandstone Helvetiafjellet Formation, which is located >70 m beneath the surface at the site (ca. 60 m below the Adventdalen sediment fill, e.g., Ogata et al., 2014), although the possibility of a deeper source (e.g., the Triassic to Early Jurassic fractured sandstone Geerdalen Formation; Mulrooney et al., 2018) could not be excluded. Sandstone, in particular, fractured, usually has a high water:rock ratio, as well as a low thorium content, compared with the silt-dominated sediments that comprise the valley infill. Sandstone could also explain the limited water-rock interaction, which is demonstrated by the similarity to seawater composition in the ADE-2 ground ice (Fig. 4). Logs taken at deep boreholes in Adventdalen, albeit closer (5 km) to the sea, indicated that groundwater salinity in the Helvetiafjellet Formation (and deeper) is ≥20 mS/cm (~40% seawater conductivity; Braathen et al., 2012), which could also be the case in the basement rocks beneath the ADE site. We note that, as suggested earlier, the proposed water intrusion could as well be a continuous process, which could start earlier during the Holocene, but its main impact should be relatively recent in order to keep that ground ice ^{226}Ra relatively low.

The ascent of water from the sub-permafrost zone is demonstrated in Svalbard by artesian discharge, associated with the common pingo structures (e.g., Demidov et al., 2019; Hodson et al., 2020; Rotem et al., 2024). This discharge is controlled either by hydraulic heads from the surrounding mountains or by basal permafrost aggradation (e.g., Hornum et al., 2020). Intra-permafrost intrusion or segregation events were also documented in various environments (e.g., French, 2007; Weinstein et al., 2019), sometimes related to non-frozen cryopeg lenses (e.g., Stephani et al., 2020; Iwahana et al., 2021). Although not a massive ice body, like in the common segregated and intrusive ice (e.g., Humlum et al., 2003; Demidov et al., 2021), it is proposed that the relatively 'young' (<2000 years) ground ice of ADE-2 was formed by saline fluids that arrived from the underlying sandstone reservoir (Fig. 1312), possibly forced by the same hydraulic pressure that drives artesian discharge in the nearby pingos (e.g., Hornum et al., 2020). These fluids have been emplaced (intruded) and mixed with ground- ice in the shallower permafrost zone in a fingering style, which resulted in the local heterogeneity at the ADE site.

We note that since ground ice analysis has been performed on large core segments (length >0.5 m) and considering the very variable salinity (e.g., 2,000 to >20,000 mgCl l^{-1} in the epigenetic zone, depth of 5-15 m from the surface, Fig. 3a), we do not have a good resolution of the actual distribution of the saline ground ice distribution. Accordingly, it could as well be that the high salinity observed is in fact due to small pockets of higher salinity, where the fingering intrusive fluids managed to intrude pore space. We also have no indication of the intrusion pathways, which should be further studied.

5.4 The ^{224}Ra/^{228}Ra enigma

The relatively low daughter-parent (^{224}Ra/^{228}Ra)$_{AR}$ ratios (<<1) in permafrost ground ice have been noticed in several cases (Weinstein et al., (2019, in Svalbard, ; Kipp et al., (2025), in Arctic Canada, ; and Zhang et al., (2025)2025, worldwide). This is remarkably different from the common steady statesteady-state ratios of 1-2, mentioned in most groundwater publications (e.g., Krishnaswami et al., 1982; Davidson and Dickson, 1986; Kiro et al., 2015). Interestingly, low ratios also appear in deep, old brines from coastal Israel (Weinstein et al., 2021). In both cases, this was attributed to the adsorption of ^{228}Th (direct ^{224}Ra parent, ^{228}Ra daughter) onto grain surfaces or aquifer rocks, thereby retaining some of the produced ^{224}Ra on the grains and preventing it from reaching the pore space fluid/ice. This, in turn, required the presence of some non-frozen fluid in the pore space, probably as thin films around the grains, in order to allow the highly particle-reactive thorium to adsorb onto grain surfaces. This which is in agreement with the observed partially frozen nature of the permafrost in Svalbard and elsewhere (e.g., Keating et al., 2018; Weinstein et al., 2019).

Nevertheless, the results of this study (Fig. 9) suggest that this is not an across-the-board observation, and that some of the samples show ratios within the 'expected' range of 1-2, although this could be affected by enhanced desorption during sample processing in the lab. This is in particular observed in the deep, epigenetic samples of ADE-2, which could be related to the higher salinity (i.e. less adsorption or enhanced desorption) in these samples. Considering the much lower half-lives involved (5.75 years for ^{228}Ra, days for ^{224}Ra), the difference in age between the cores does not seem relevant to the ^{224}Ra/^{228}Ra ratios. On the other hand, it could have to do with the higher salinity in ADE-2, which could result in less adsorption of ^{228}Th and should be further studied.

6. Summary and Conclusions

In this paper, we used both chemistry and Ra and Th isotopes to get an insight into the ~~intra-permafrost~~ ground ice history and fluid migration in the continuous permafrost of a Svalbard valley. While the dominant control on the contribution of short-lived Ra isotopes into the pore space is the recoil of Th-parent nuclides residing on the soil grain surfaces, the supply of the long-lived ^{226}Ra is also controlled by slow diffusion out of the soil grains, probably mainly through frozen nano-pores. ~~These are superimposed by adsorption, which is related to the common presence of fluid in the cryotic pore space of the saline permafrost, and which affects similarly both radium isotope activities and the time of reaching secular equilibrium.~~The actual activities of both are also controlled by adsorption, which in turn is dependent on the existence of liquid water in the pore space under the discussed cryotic conditions. -The relatively low $(^{226}Ra/^{sl}Ra)_{AR}$ in the ground ice of one core (ADE-2) and its equilibrium with grain surface ratios of thorium isotope parents, while the much higher Ra isotope ratios in the other two cores (ADE-17 and ADE-1), suggest that ground ice in the first is younger, or more precisely – has been recently regenerated, ~~,~~ probably ~~related to recent~~as a result of fluid intrusion, either as a single or a continuous event, and Ra isotope clock reset. This fluid was significantly more saline than the original one, as reflected in the higher salinity of this core's ground ice, compared with the other cores. Salinization goes almost all the way to the surface, also demonstrating its recent history. The similarity to seawater composition ~~in~~ of this young ground ice suggests that the intruding fluids were less subjected to WRI, which is probably due to the characteristic higher water:rock ratio of its source aquifer, most likely ~~the~~ an underlying sandsto~~m~~ne formation~~local basement~~. On the other hand, the different from seawater composition in the other two cores suggests that the water had a significantly longer history in the valley-fill sediments prior to freezing, which is in accordance with their suggested longer residence time.

This study demonstrates the heterogeneity of the saline permafrost and highlights its complex history and liability to fluid migration, which is probably also the case in other permafrost terrains. This further highlights saline permafrost's vulnerability to the ongoing climate change and warming. As Arctic temperatures continue to rise, the degradation of saline permafrost may trigger or enh~~e~~ance subsurface fluid mobilization~~and destabilization~~, posing significant risks to infrastructure and accelerating the release of stored carbon ~~in~~to the atmosphere.

Appendices

Tables C1, C2 and C3

Table C1. Chemistry and ice content* of ground ice in the ADE cores, East Adventdalen

Sample	permafrost type	depth	Cl^-	Br^-	SO_4^{--}	SiO_2	Na^+	K^+	Sr^{++}	Ca^{++}	Mg^{++}	HCO_3^-	ice content
ADE-17	-	M	mg l^{-1}	mg l^{-1}	mg l^{-1}	mg l^{-1}	mg l^{-1}	mg l^{-1}	mg l^{-1}	mg l^{-1}	mg l^{-1}	mg l^{-1}	%
DR-AD-55	Syngenetic	1.3	27.3	0.5	23.5	12.8	11.3	18.1	0.20	5.5	15.5	—	165
DR-AD-58	Syngenetic	2.1	12.7	0.6	29.7	14.0	19.7	3.8	0.41	8.8	27.8	—	69
DR-AD-52	Syngenetic	2.9	72.1	0.7	24.1	8.8	15.5	46.9	0.61	12.6	35.3	—	88
DR-AD-57	Syngenetic	3.3	14.0	0.5	29.1	5.9	32.6	4.8	0.13	3.6	7.7	—	170
DR-AD-56	Syngenetic	3.5	9.9	0.3	11.8	5.3	13.2	4.4	0.07	1.5	2.6	—	149
DR-AD-61	Syngenetic	4.0	14.5	0.7	13.0	11.6	9.5	5.2	0.16	3.6	8.8	—	100
DR-AD-63	Syngenetic	4.1	26.8	—	13.4	29.8	13.0	14.1	0.13	1.7	2.8	—	131
DR-AD-59	Syngenetic	5.5	65.3	0.6	156.5	19.9	81.2	20.6	0.51	13.5	27.8	—	105
DR-AD-53	Epigenetic	6.3	468.3	2.1	102.4	20.5	449.9	0.7	0.53	14.5	3.6	—	14
DR-AD-64	Epigenetic	6.5	765.3	—	362.5	34.7	750.3	29.1	0.15	11.5	—	—	27
DR-AD-65	Epigenetic	8.1	1491.1	—	446.3	19.3	1154.4	35.6	0.08	1.7	—	—	22
DR-AD-54	Epigenetic	9.4	1896.9	7.0	483.7	8.5	2209.7	181.9	0.30	16.3	—	—	21
DR-AD-66	Epigenetic	9.8	3229.6	—	704.6	23.2	2498.3	45.8	0.34	9.7	—	—	10
DR-AD-60	Epigenetic	11.8	2246.3	6.6	400.5	19.4	2161.1	97.1	0.53	17.8	—	—	14
ADE-1													
DR-AD-146	Syngenetic	4.1	20.0	—	34.8	6.0	17.0	2.9	0.15	7.0	3.1	9.0	182
DR-AD-147	Syngenetic	4.9	—	0.8	139.8	12.9	84.4	13.7	0.67	36.6	17.4	35.1	87
DR-AD-128	Epigenetic	5.7	445.0	1.9	41.8	8.0	270.0	23.6	0.37	21.6	16.4	85.1	35
DR-AD-129	Epigenetic	6.1	902.0	3.7	176.0	10.2	626.0	57.1	0.45	25.5	25.0	232.1	22
DR-AD-130	Epigenetic	6.4	1157.3	4.2	261.5	10.1	866.9	50.1	0.21	10.5	16.4	197.6	45
DR-AD-131	Epigenetic	6.9	1226.4	4.3	468.6	9.6	1012.7	42.4	0.16	7.7	10.9	143.6	27
DR-AD-149	Epigenetic	7.9	2348.7	5.6	1418.0	4.0	2043.6	98.2	0.51	19.4	30.6	227.2	17
DR-AD-123	Epigenetic	10.1	1275.6	4.0	200.3	9.6	961.3	8.8	0.04	0.7	—	183.9	16
DR-AD-148	Epigenetic	11.0	1718.7	4.2	978.9	7.7	1434.4	90.8	0.50	18.5	24.6	195.2	29
ADE-2													
DR-AD-145	Syngenetic	5.2	5010.0	119.1	1548.8	8.6	3259.8	241.5	2.57	122.6	176.3	243.0	23
DR-AD-126	Epigenetic	6.2	5035.7	17.3	465.9	9.3	3209.7	152.8	1.45	61.8	128.9	151.0	23
DR-AD-132	Epigenetic	7.6	7079.1	24.6	445.7	7.6	4240.9	223.3	2.85	102.4	234.2	45.9	13
DR-AD-125	Epigenetic	8.4	23194.9	78.9	801.9	20.6	14624.5	367.0	6.03	222.2	366.6	611.9	2
DR-AD-124	Epigenetic	9.9	4616.5	15.8	573.7	7.8	3041.5	156.1	1.69	62.4	110.5	164.5	45
DR-AD-150	Epigenetic	10.9	6521.9	17.6	2094.9	29.3	3928.9	2487.8	—	1.4	7.9	340.4	13
DR-AD-122	Epigenetic	11.7	5420.0	17.8	631.5	11.5	3552.7	160.2	2.29	85.2	115.2	239.3	12
DR-AD-133	Epigenetic	12.3	7071.5	26.0	724.5	7.2	4129.4	215.9	4.50	164.3	268.5	66.7	116
DR-AD-151	Epigenetic	12.9	7961.7	22.0	2729.2	7.3	5329.8	377.7	6.61	240.8	292.6	222.5	20
DR-AD-134	Epigenetic	13.9	2774.2	8.2	266.9	6.3	1505.5	75.8	2.57	77.2	106.7	—	13
DR-AD-121	Epigenetic	14.6	4474.1	14.5	333.9	9.9	2679.3	107.9	4.07	91.3	106.1	191.3	25

*ice content = ice/dry weight

Sample	permafrost type	depth	Cl^-	Br^-	SO_4^{--}	SiO_2	Na^+	K^+	Sr^{++}	Ca^{++}	Mg^{++}	HCO_3^-	ice content*
ADE-17	-	m	mg l^{-1}	mg l^{-1}	mg l^{-1}	mg l^{-1}	mg l^{-1}	mg l^{-1}	mg l^{-1}	mg l^{-1}	mg l^{-1}	mg l^{-1}	%
DR-AD-55	Syngenetic	1.3	27.3	0.5	23.5	12.8	11.3	18.1	0.2	5.5	15.5	---	165
DR-AD-58	Syngenetic	2.1	12.7	0.6	29.7	14	19.7	3.8	0.41	8.8	27.8	---	69
DR-AD-52	Syngenetic	2.9	72.1	0.7	24.1	8.8	15.5	46.9	0.61	12.6	35.3	---	88
DR-AD-57	Syngenetic	3.3	14	0.5	29.1	5.9	32.6	4.8	0.13	3.6	7.7	---	170
DR-AD-56	Syngenetic	3.5	9.9	0.3	11.8	5.3	13.2	4.4	0.07	1.5	2.6	---	149
DR-AD-61	Syngenetic	4.0	14.5	0.7	13	11.6	9.5	5.2	0.16	3.6	8.8	---	100
DR-AD-63	Syngenetic	4.1	26.8	---	13.4	29.8	13	14.1	0.13	1.7	2.8	---	131
DR-AD-59	Syngenetic	5.5	65.3	0.6	156.5	19.9	81.2	20.6	0.51	13.5	27.8	---	105
DR-AD-53	Epigenetic	6.3	468.3	2.1	102.4	20.5	449.9	0.7	0.53	14.5	3.6	---	14
DR-AD-64	Epigenetic	6.5	765.3	---	362.5	34.7	750.3	29.1	0.15	11.5	---	---	27
DR-AD-65	Epigenetic	8.1	1491.1	---	446.3	19.3	1154.4	35.6	0.08	1.7	---	---	22
DR-AD-54	Epigenetic	9.4	1896.9	7	483.7	8.5	2209.7	181.9	0.3	16.3	---	---	21
DR-AD-66	Epigenetic	9.8	3229.6	---	704.6	23.2	2498.3	45.8	0.34	9.7	---	---	10
DR-AD-60	Epigenetic	11.8	2246.3	6.6	400.5	19.4	2161.1	97.1	0.53	17.8	---	---	14
ADE-1													
DR-AD-146	Syngenetic	4.1	20	---	34.8	6	17	2.9	0.15	7	3.1	9	182
DR-AD-147	Syngenetic	4.9	---	0.8	139.8	12.9	84.4	13.7	0.67	36.6	17.4	35.1	87
DR-AD-128	Epigenetic	5.7	445	1.9	41.8	8	270	23.6	0.37	21.6	16.4	85.1	35
DR-AD-129	Epigenetic	6.1	902	3.7	176	10.2	626	57.1	0.45	25.5	25	232.1	22
DR-AD-130	Epigenetic	6.4	1157.3	4.2	261.5	10.1	866.9	50.1	0.21	10.5	16.4	197.6	45
DR-AD-131	Epigenetic	6.9	1226.4	4.3	468.6	9.6	1012.7	42.4	0.16	7.7	10.9	143.6	27
DR-AD-149	Epigenetic	7.9	2348.7	5.6	1418	4	2043.6	98.2	0.51	19.4	30.6	227.2	17
DR-AD-123	Epigenetic	10.1	1275.6	4	200.3	9.6	961.3	8.8	0.04	0.7	---	183.9	16
DR-AD-148	Epigenetic	11.0	1718.7	4.2	978.9	7.7	1434.4	90.8	0.5	18.5	24.6	195.2	29
ADE-2													
DR-AD-142	Syngenetic	3.5	827.6	2.4	291.2	16.1	204.6	---	3.6	228.3	70.2	8.3	108
DR-AD-141	Syngenetic	4.4	2778.7	5.9	1320.2	8.2	1756.9	59.8	4.1	218.8	156.3	10.9	108
DR-AD-145	Syngenetic	5.2	5010	119.1	1548.8	8.6	3259.8	241.5	2.57	122.6	176.3	243	23
DR-AD-126	Epigenetic	6.2	5035.7	17.3	465.9	9.3	3209.7	152.8	1.45	61.8	128.9	151	23
DR-AD-132	Epigenetic	7.6	7079.1	24.6	445.7	7.6	4240.9	223.3	2.85	102.4	234.2	45.9	13
DR-AD-125	Epigenetic	8.4	23194.9	78.9	801.9	20.6	14624.5	367	6.03	222.2	366.6	611.9	2
DR-AD-124	Epigenetic	9.9	4616.5	15.8	573.7	7.8	3041.5	156.1	1.69	62.4	110.5	164.5	45
DR-AD-150	Epigenetic	10.9	6521.9	17.6	2094.9	29.3	3928.9	2487.8	---	1.4	7.9	340.4	13
DR-AD-122	Epigenetic	11.7	5420	17.8	631.5	11.5	3552.7	160.2	2.29	85.2	115.2	239.3	12
DR-AD-133	Epigenetic	12.3	7071.5	26	724.5	7.2	4129.4	215.9	4.5	164.3	268.5	66.7	116
DR-AD-151	Epigenetic	12.9	7961.7	22	2729.2	7.3	5329.8	377.7	6.61	240.8	292.6	222.5	20
DR-AD-134	Epigenetic	13.9	2774.2	8.2	266.9	6.3	1505.5	75.8	2.57	77.2	106.7	---	13
DR-AD-121	Epigenetic	14.6	4474.1	14.5	333.9	9.9	2679.3	107.9	4.07	91.3	106.1	191.3	25

*ice content = ice/dry weight

810

Table C2. Radium isotope activities* and ratios in ground ice, ADE cores.

sample	permafrost type	depth	^{223}Ra	^{224}Ra	^{226}Ra	^{228}Ra	$^{226}Ra/^{223}Ra$	$^{226}Ra/^{224}Ra$	$^{226}Ra/^{228}Ra$	$^{224}Ra/^{228}Ra$
ADE-17	-	m	dpm l^{-1}	dpm l^{-1}	dpm l^{-1}	dpm l^{-1}	-	-	-	-
DR-AD-55	Syngenetic	1.3	0.07	1.46	3.26	9.53	44.7	2.2	0.3	0.15
DR-AD-58	Syngenetic	2.1	—	—	—	—	125.0	—	—	—
DR-AD-52	Syngenetic	2.9	0.18	2.16	4.13	10.11	23.3	1.9	0.4	0.21
DR-AD-57	Syngenetic	3.3	0.02	0.13	2.71	0.99	122.0	20.3	2.7	0.13
DR-AD-56	Syngenetic	3.5	—	—	—	—	58.2	—	—	—
DR-AD-61	Syngenetic	4.0	—	—	—	—	24.0	—	—	—
DR-AD-63	Syngenetic	4.1	0.11	1.89	5.01	3.04	43.6	2.6	1.6	0.62
DR-AD-59	Syngenetic	5.5	0.06	0.50	1.44	9.00	25.7	2.9	0.2	0.06
DR-AD-53	Epigenetic	6.3	0.21	5.02	6.90	7.41	33.0	1.4	0.9	0.68
DR-AD-64	Epigenetic	6.5	0.23	2.13	16.54	16.71	72.2	7.8	1.0	0.13
DR-AD-65	Epigenetic	8.1	1.02	12.88	56.49	20.44	55.4	4.4	2.8	0.63
DR-AD-67	Epigenetic	8.8	0.32	7.04	13.24	—	41.6	1.9	—	—
DR-AD-54	Epigenetic	9.4	0.23	3.10	3.74	16.67	16.0	1.2	0.2	0.19
DR-AD-66	Epigenetic	9.8	0.27	3.83	15.78	18.88	57.7	4.1	0.8	0.20
DR-AD-60	Epigenetic	11.8	0.20	2.60	3.60	27.56	18.0	1.4	0.1	0.09
ADE-1	-	-	-	-	-	-	-	-	-	-
DR-AD-146	Syngenetic	4.1	0.03	0.59	2.96	—	109.2	5.0	—	—
DR-AD-147	Syngenetic	4.9	0.10	0.85	3.87	—	39.0	4.5	—	—
DR-AD-149	Epigenetic	7.9	—	—	—	—	14.7	—	—	—
DR-AD-123	Epigenetic	10.1	0.19	2.12	6.26	—	32.5	3.0	—	—
DR-AD-148	Epigenetic	11.0	—	—	—	—	14.4	—	—	—
ADE-2	-	-	-	-	-	-	-	-	-	-
DR-AD-145	Syngenetic	5.2	1.03	18.95	14.47	—	14.1	0.8	—	—
DR-AD-126	Epigenetic	6.2	0.64	8.44	4.49	15.28	7.0	0.5	0.3	0.55
DR-AD-125	Epigenetic	8.4	1.87	27.57	26.56	25.50	14.2	1.0	1.0	1.08
DR-AD-124	Epigenetic	9.9	0.86	8.81	6.36	14.84	7.4	0.7	0.4	0.59
DR-AD-150	Epigenetic	10.9	1.45	24.64	10.95	—	7.6	0.4	—	—
DR-AD-122	Epigenetic	11.7	0.76	10.83	8.39	6.84	11.0	0.8	1.2	1.58
DR-AD-151	Epigenetic	12.9	3.92	58.66	14.99	—	3.8	0.3	—	—
DR-AD-121	Epigenetic	14.6	0.94	18.24	5.32	12.16	5.7	0.3	0.4	1.50

sample	permafrost type	depth	^{223}Ra	^{224}Ra	^{226}Ra	^{228}Ra	$^{226}Ra/^{223}Ra$	$^{226}Ra/^{224}Ra$	$^{226}Ra/^{228}Ra$	$^{224}Ra/^{228}Ra$
ADE-17		m	dpm l^{-1}	dpm l^{-1}	dpm l^{-1}	dpm l^{-1}	-			
DR-AD-55	Syngenetic	1.3	0.07±0.03	1.46±0.15	3.26±0.20	9.53±0.52	44.7±17.3	2.2±0.27	0.3±0.03	0.15±0.02
DR-AD-52	Syngenetic	2.9	0.18±0.04	2.16±0.19	4.13±0.25	10.11±0.54	23.33±5.8	1.9±0.2	0.4±0.03	0.21±0.02
DR-AD-57	Syngenetic	3.3	0.02±0.01	0.13±0.01	2.71±0.16	0.99±0.05	122.00±39.9	20.3±2.4	2.7±0.2	0.13±0.02
DR-AD-56	Syngenetic	3.5	---	---	---	---	18.08±6.8	---	---	---
DR-AD-61	Syngenetic	4.0	---	---	---	---	24.00±5.8	---	---	---
DR-AD-63	Syngenetic	4.1	0.11±0.02	1.89±0.13	5.01±0.29	3.04±0.16	43.62±7.6	2.6±0.2	1.6±0.1	0.62±0.05
DR-AD-59	Syngenetic	5.5	0.06±0.02	0.50±0.05	1.44±0.09	9.00±0.51	25.67±7.7	2.9±0.3	0.2±0.01	0.06±0.01
DR-AD-53	Epigenetic	6.3	0.21±0.07	5.02±0.50	6.90±0.41	7.41±0.39	33.05±12.0	1.4±0.2	0.9±0.07	0.68±0.08
DR-AD-64	Epigenetic	6.5	0.23±0.07	2.13±0.23	16.54±0.96	16.71±0.83	72.2±22.6	7.8±0.9	1.0±0.08	0.13±0.02
DR-AD-65	Epigenetic	8.1	1.02±0.30	12.88±1.23	56.49±3.49	20.44±1.10	55.39±16.7	4.4±0.5	2.8±0.23	0.63±0.07
DR-AD-67	Epigenetic	8.8	0.32±0.14	7.04±0.75	13.24±0.82	---	41.6±18.9	1.9±0.2	---	---
DR-AD-54	Epigenetic	9.4	0.23±0.08	3.10±0.30	3.74±0.21	16.67±0.94	16.0±5.2	1.2±0.1	0.2±0.02	0.19±0.02
DR-AD-66	Epigenetic	9.8	0.27±0.09	3.83±0.41	15.78±0.98	18.88±0.79	57.7±19.9	4.1±0.5	0.8±0.06	0.20±0.02
DR-AD-60	Epigenetic	11.8	0.20±0.06	2.60±0.23	3.60±0.24	27.56±1.64	18.0±5.7	1.4±0.1	0.1±0.01	0.09±0.01
ADE-1										
DR-AD-146	Syngenetic	4.1	0.03±0.01	0.59±0.05	2.96±0.17	---	109.2±37.5	5.0±0.5	---	---
DR-AD-147	Syngenetic	4.9	0.10±0.03	0.85±0.09	3.87±0.22	---	39.0±10.9	4.5±0.5	---	---
DR-AD-149	Epigenetic	7.9	---	---	---	---	14.7±3.8	---	---	---
DR-AD-123	Epigenetic	10.1	0.19±0.08	2.12±0.28	6.26±0.35	---	32.5±13.5	3.0±0.4	---	---
DR-AD-148	Epigenetic	11.0	---	---	---	---	14.4±4.0	---	---	---
ADE-2										
DR-AD-145	Syngenetic	5.2	1.20±0.24	22.15±2.04	14.68±0.86	---	12.25±2.5	0.6±0.07	---	---
DR-AD-126	Epigenetic	6.2	0.64±0.13	8.44±0.69	4.49±0.24	15.28±0.96	7.0±1.5	0.5±0.05	0.3±0.02	0.55±0.06
DR-AD-125	Epigenetic	8.4	1.78±0.46	30.24±2.16	26.56±1.48	25.50±1.13	14.9±3.9	0.9±0.08	1.0±0.07	1.2±0.1
DR-AD-124	Epigenetic	9.9	0.86±0.15	8.81±0.63	6.36±0.34	14.84±0.73	7.4±1.3	0.7±0.06	0.4±0.03	0.59±0.05
DR-AD-150	Epigenetic	10.9	1.45±0.30	24.64±1.84	10.95±0.64	---	7.6±1.6	0.4±0.04	---	---
DR-AD-122	Epigenetic	11.7	0.76±0.12	10.83±0.83	8.39±0.48	6.84±0.23	11.0±1.9	0.8±0.07	1.2±0.08	1.58±0.1
DR-AD-151	Epigenetic	12.9	4.15±0.53	58.66±4.25	14.99±0.90	---	3.6±0.5	0.3±0.02	---	---
DR-AD-121	Epigenetic	14.6	0.94±0.20	18.24±1.40	5.32±0.28	12.16±0.35	5.7±1.2	0.3±0.03	0.4±0.03	1.50±0.1

*Activities are not presented for samples with Ra adsorption efficiencies lower than 50%.

Table C3. Thorium isotopes activities and ^{227}Ac in sediments from ADE-17

sample	permafrost type	depth	^{232}Th	^{230}Th	^{228}Th	^{227}Ac	^{232}Th	^{230}Th	^{228}Th	^{227}Ac	$^{230}Th/^{227}Ac$	$^{230}Th/^{227}Ac$	$^{230}Th/^{228}Th$	$^{230}Th/^{228}Th$	$^{230}Th/^{232}Th$	$^{230}Th/^{232}Th$
-	-	m	dpm g^{-1}	dpm g^{-1}	dpm g^{-1}	dpm g^{-1}	dpm g^{-1}	dpm g^{-1}	dpm g^{-1}	dpm g^{-1}	-	-	-	-	-	-
-	-	-	bulk sediment				CEC				bulk	CEC	bulk	CEC	bulk	CEC
DR-AD-51	Active layer	0.5	5.3	4.5	0.7	0.02	0.12	0.06	0.28	0.02	267	3.4	6.4	0.22	0.86	0.53
DR-AD-55	Syngenetic	1.3	5.5	4.3	1.0	0.06	0.03	0.02	0.08	0.01	79	2.6	4.4	0.23	0.79	0.69
DR-AD-58	Syngenetic	2.1	6.8	4.7	0.9	0.08	0.13	0.07	0.14	---	62	---	5.5	0.51	0.70	0.55
DR-AD-57	Syngenetic	3.3	6.8	5.2	0.6	0.07	0.06	0.04	0.15	0.01	78	6.2	9.2	0.25	0.76	0.60
DR-AD-61	Syngenetic	4.0	6.4	5.3	0.4	0.03	0.17	0.10	0.23	---	191	---	12.4	0.43	0.83	0.57
DR-AD-63	Syngenetic	4.1	6.3	5.2	0.6	0.07	0.11	0.07	1.20	0.01	71	7.7	9.0	0.06	0.83	0.61
DR-AD-59	Syngenetic	5.5	4.9	5.0	0.5	0.06	0.07	0.05	0.45	---	83	---	10.1	0.11	1.02	0.75
DR-AD-64	Epigenetic	6.5	7.9	7.6	0.3	---	0.04	0.05	0.10	0.01	---	5.2	24.4	0.54	0.95	1.33
DR-AD-67	Epigenetic	8.8	7.8	7.1	0.4	0.07	0.01	0.02	0.61	0.01	100	1.9	19.2	0.03	0.91	1.75
DR-AD-54	Epigenetic	9.4	8.4	7.0	0.7	0.04	0.10	0.17	0.29	0.02	185	8.5	9.8	0.58	0.84	1.69
DR-AD-60	Epigenetic	11.8	5.9	5.9	0.4	0.02	0.06	0.10	0.27	0.02	371	4.9	15.6	0.38	1.00	1.61

Table C3. Thorium isotopes activities and ^{227}Ac in sediments from ADE-17

sample	PF type	depth	^{232}Th	^{230}Th	^{228}Th	^{227}Ac	^{232}Th	^{230}Th	^{228}Th	^{227}Ac	$^{230}Th/^{227}Ac$	$^{230}Th/^{227}Ac$	$^{230}Th/^{228}Th$	$^{230}Th/^{228}Th$	$^{230}Th/^{232}Th$	$^{230}Th/^{232}Th$
			dpm g^{-1}	dpm g^{-1}	dpm g^{-1}	dpm g^{-1}	dpm g^{-1}	dpm g^{-1}	dpm g^{-1}	dpm g^{-1}						
		m	bulk sediment				exchangeable fraction				bulk	exchangeable	bulk	exchangeable	bulk	exchangeable
DR-AD-51	AC	0.5	5.32	4.55	0.85±0.07	0.03±0.01	0.12	0.06	0.26±0.02	0.021±0.004	134±51	2.9±0.5	5.4±0.5	0.24±0.01	0.86	0.53
DR-AD-55	Syn	1.3	5.53	4.35	0.77±0.06	0.05±0.01	0.03	0.02	0.07±0.01	0.007±0.003	86±22	2.7±1.0	5.7±0.4	0.27±0.03	0.79	0.69
DR-AD-58	Syn	2.1	6.82	4.75	0.78±0.06	0.09±0.02	0.13	0.07	0.04±0.00	0.003±0.001	50±11	25.9±6.6	6.1±0.5	1.94±0.15	0.70	0.55
DR-AD-57	Syn	3.3	6.83	5.19	0.71±0.06	0.06±0.01	0.06	0.04	0.15±0.01	0.005±0.001	85±21	7.7±2.2	7.3±0.6	0.25±0.02	0.76	0.60
DR-AD-61	Syn	4.0	6.43	5.34	0.53±0.05	0.03±0.01	0.17	0.10	0.28±0.02	0.010±0.001	179±52	10.2±2.1	10.0±0.9	0.35±0.02	0.83	0.57
DR-AD-63	Syn	4.1	6.31	5.23	0.88±0.08	0.08±0.03	0.11	0.07	0.23±0.01	0.012±0.003	66±21	5.91±1.3	5.9±0.5	0.29±0.02	0.83	0.61
DR-AD-59	Syn	5.5	4.90	4.99	0.58±0.05	0.06±0.02	0.07	0.05	0.04±0.00	0.003±0.001	86±23	19.3±5.9	8.7±0.7	1.35±0.11	1.02	0.75
DR-AD-64	Epi	6.5	7.94	7.57	0.31±0.05	—	0.04	0.05	0.19±0.01	0.015±0.002	—	3.6±0.4	24.6±4.1	0.27±0.02	0.95	1.33
DR-AD-67	Epi	8.8	7.75	7.09	0.35±0.05	0.07±0.03	0.01	0.02	0.16±0.01	0.011±0.002	99±37	1.8±0.3	20.1±2.9	0.13±0.01	0.91	1.75
DR-AD-54	Epi	9.4	8.41	7.03	0.66±0.06	0.03±0.01	0.10	0.17	0.19±0.01	0.014±0.002	271±122	12.5±1.9	10.7±0.9	0.88±0.05	0.84	1.69
DR-AD-60	Epi	11.8	5.94	5.93	0.34±0.04	0.02±0.01	0.06	0.10	0.15±0.01	0.009±0.002	364±211	11.0±2.1	17.3±2.1	0.68±0.04	1.00	1.61

PF = permafrost, AC = Active Layer, Syn and Epi = Syngenetic and Epigenetic permafrost respectively

Data availability

Data is available through DOI: 10.6084/m9.figshare.30959015

Author contribution

DR, YW, and HHC planned the drilling campaigns; DR and YW processed the cores and lab work in UNIS Svalbard; DR and YH performed the water and soil fractions chemistry analysis at GSI; AT performed soil fraction analyses at the Hebrew University lab. YW developed the simulations of radium isotopes diffusion from sediment clay grains into the pore space; DR and YW wrote the manuscript. All authors commented on the manuscript.

Competing interests

The authors declare that they have no conflict of interest.

Acknowledgments

We would like to express our gratitude to Ullrich (Ulli) Neuman for leading the 2017 and 2022 drilling campaigns in Adventdalen. Many thanks to Andreas Alexander and Graham L. Gilbert for field assistance, to Danni Rohdent and Mai-Brit Schulte for assistance in the lab, and to Gerd-Irene Sigernes and the UNIS logistics personnel for their great assistance with field and laboratory gear. We are also very thankful to the GSI researchers and technicians Olga Berlin, Galit Sharabi, Dina Shtiber, Keren Weiss, and Anton Vaks, who helped with chemical and Th isotope analysis.

Financial support

The project was funded by the Israel Science Foundation grant ISF163/19, while the drilling campaigns were also supported by an Arctic Field Grant from the Norwegian Research Council, Project Number: 269988 RiS ID: 10664.

References

Abramov, A., Vishnivetskaya, T., and Rivkina, E.: Are permafrost microorganisms as old as permafrost? FEMS Microbiol. Ecol, 97(2). https://doi.org/10.1093/femsec/fiaa260, 2021.

Ahonen, L.: Permafrost: occurrence and physiochemical processes (POSIVA--01-05). POSIVA OY, Finland, 2001.

Åkerman, H. J., and Malmström, B.: Permafrost Mounds in the Abisko Area, Northern Sweden. Geografiska Annaler: Series A, Physical Geography, 68(3), 155–165. https://doi.org/10.1080/04353676.1986.11880169, 1986.

Alekseyev, V.R.: Cryogenesis and geodynamics of icing valleys. Geodyn. Tectonophys. 6 (2), 171–224. https://doi.org/10.5800/GT-2015-6-2-0177, 2015.

Anisimov, O. A., and Nelson, F. E.: Permafrost zonation and climate change in the northern hemisphere: results from transient general circulation models. Clim. Change, 35(2), 241-258. https://doi.org/10.1023/A:1005315409698, 1986.

Banin, A., and Anderson, D. M.: Effects of Salt Concentration Changes During Freezing on the Unfrozen Water Content of Porous Materials. Water Resour. Res, *10*(1), 124-128. https://doi.org/10.1029/WR010i001p00124, 1974.

Boike, J., Roth, K., and Overduin, P. P.: Thermal and hydrologic dynamics of the active layer at a continuous permafrost site (Taymyr Peninsula, Siberia). Water Resour. Res., 34(3), 355-363. https://doi.org/10.1029/97WR03498, 1998.

Braathen, A., Bælum, K., Christiansen, H.H., et al.: The Longyearbyen CO_2 Lab of Svalbard, Norway—initial assessment of the geological conditions for CO_2 sequestration. Nor. J. Geol., Vol 92, pp. 353–376. Trondheim 2012, ISSN 029-196X, 2012.

Brady, J. B., and Cherniak, D. J.: Diffusion in Minerals: An Overview of Published Experimental Diffusion Data. Rev. Mineral. Geochem., 72, 899–920. https://doi.org/10.2138/rmg.2010.72.20, 2010.

Brigham-Grette, J., and Hopkins, D. M.: Emergent Marine Record and Paleoclimate of the Last Interglaciation along the Northwest Alaskan Coast. Quat. Res., 43(2), 159-173, 1995.

Brouchkov, A.: Nature and distribution of frozen saline sediments on the Russian Arctic coast. Permafr. Periglac. Process, 13, 83–90. https://doi.org/10.1006/qres.1995.1017, 2002.

Brown, J., O. Ferrians, J. A. Heginbottom, E., and Melnikov, E.S.: Circum-Arctic Map of Permafrost and Ground-Ice Conditions, Version 2 [Data Set]. Boulder, Colorado, USA. National Snow and Ice Data Center, 2002.

Bullock, E. J., Kipp, L., Moore, W., Brown, K., Mann, P. J., Vonk, J. E., Zimov, N., and Charette, M. A.: Radium Inputs Into the Arctic Ocean From Rivers: A Basin-Wide Estimate. Journal of Geophysical Research: Oceans, 127(9), e2022JC018964. https://doi.org/10.1029/2022JC01896, (2022).

Burn, C. R., & Michel, F. A.: Evidence for recent temperature-induced water migration into permafrost from the tritium content of ground ice near Mayo, Yukon Territory, Canada. Canadian Journal of Earth Sciences, 25(6), 909-915. https://doi.org/10.1139/e88-087, 1988.

Cable, S., Elberling, B., and Kroon, A.: Holocene permafrost history and cryostratigraphy in the High-Arctic Adventdalen Valley, central Svalbard. Boreas, 47(2), 423-442. https://doi.org/10.1111/bor.12286, 2018.

Cherniak, D.J.: Cation Diffusion in Feldspars. Reviews in Mineralogy & Geochemistry 72, 691-733. DOI: 10.2138/rmg.2010.72.15, 2010.

Charkin, A. N., Pipko, I. I., Yu. Pavlova, G., Dudarev, O. V., Leusov, A. E., Barabanshchikov, Y. A., Shcherbakova, K. P., Yaroshchuk, E. I., Pugach, S. P., Gulenko, T. A., Goriachev, V. A., Semiletov, I. P., and Zarubina, N. V.: Hydrochemistry and isotopic signatures of sub-permafrost groundwater discharge along the eastern slope of the Lena River Delta in the Laptev Sea. Journal of Hydrology, 590, 125515. https://doi.org/10.1016/j.jhydrol.2020.125515, 2020.

Christiansen, H. H., French, H. M., and Humlum, O.: Permafrost in the Gruve-7 mine, Adventdalen, Svalbard. Norw. J. Geog., 59(2), 109–115. https://doi.org/10.1080/00291950510020592, 2005.

Dafflon, B., Hubbard, S., Ulrich, C., Peterson, J., Wu, Y., Wainwright, H., and Kneafsey, T. J.: Geophysical estimation of shallow permafrost distribution and properties in an ice-wedge polygon-dominated Arctic tundra region. Geophys, 81(1). https://doi.org/10.1190/geo2015-0175.1, 2016.

Dabrowski, J. S.: Radium isotopes and radon-222 as tracers of sediment-water interaction in Arctic coastal and, (2020).

Davidson, M.R., and Dickson, B.L.: A porous flow model for steady state transport of radium in groundwater. Water Resour. Res. 22 (1), 34–44, 1986.

de Baar, H.J.W., van Heuven, S.M.A.C., and Middag, R.: Ocean Salinity, Major Elements, and Thermohaline Circulation. In: White, W. (eds) Encyclopedia of Geochemistry. Encyclopedia of Earth Sciences Series. Springer, Cham, 2017.

Demidov, N., Wetterich, S., Verkulich, S., Ekaykin, A., Meyer, H., Anisimov, M., Schirrmeister, L., Demidov, V., and Hodson, A. J.: Geochemical signatures of pingo ice and its origin in Grøndalen, west Spitsbergen, The Cryosphere, 13, 3155–316. https://doi.org/10.5194/tc-13-3155-2019, 2019.

Demidov, V., Wetterich, S., Demidov, N., Schirrmeister, L., Verkulich, S., Koshurnikov, A., Gagarin, V., Ekaykin, A., Terekchov, A., Veres, A., and Kozachek, A.: Pingo drilling reveals sodium–chloride-dominated massive ice in Grøndalen, Spitsbergen. Permafr. Periglac. Process, *32*(4), 572-586. https://doi.org/10.1002/ppp.2124, 2021.

Dickinson, W.W., and Rosen, M.R.: Antarctic permafrost: An analogue for water and diagenetic minerals on Mars. Geology 31 (3): 199–202. https://doi.org/10.1130/0091-7613(2003)031<0199:APAAFW>2.0.CO;2, 2003.

Dobinski, W.: Permafrost. Earth Sci. Rev., 108(3-4), 158-169. https://doi.org/10.1016/j.earscirev.2011.06.007, 2011.

Diego-Feliu, M., Rodellas, V., Saaltink, M., Alorda-Kleinglass, A., Goyetche, T., Martínez-Pérez, L., Folch, A., & Garcia-Orellana, J.: New perspectives on the use of 224Ra/228Ra and 222Rn/226Ra activity ratios in groundwater studies. Journal of Hydrology, 596, 126043. https://doi.org/10.1016/j.jhydrol.2021.126043, 2021.

Dimova, N. T., Paytan, A., Kessler, J. D., Sparrow, K. J., Garcia-Tigreros Kodovska, F., Lecher, A. L., ... and Tulaczyk, S. M.: Current magnitude and mechanisms of groundwater discharge in the Arctic: case study from Alaska. Environmental Science and Technology, 49(20), 12036-12043. https://doi.org/10.1021/acs.est.5b02215, 2015.

Elverhøi, A., Svendsen, J. I., Solheim, A., Andersen, E. S., Milliman, J., Mangerud, J., and Hooke, R. L.: Late Quaternary Sediment Yield from the High Arctic Svalbard Area. J. Geol. 103(1). https://doi.org/10.1086/629718, 1994.

Ewing, S.A., Paces, J.B., O'Donnell, J.A., Jorgenson, M.T., Kanevskiy, M.Z., Aiken, G.R., Shur, Y., Harden, J.W., and Striegl, R.: Uranium isotopes and dissolved organic carbon in loess permafrost: modeling the age of ancient ice. Geochim. Cosmochim. Acta 152, 143–165. https://doi.org/10.1016/j.gca.2014.11.008, 2015.

Fisher, D. A., Lacelle, D., and Pollard, W.: A model of unfrozen water content and its transport in icy permafrost soils: Effects on ground ice content and permafrost stability. Permafr. Periglac. Process, 31(1), 184-199. https://doi.org/10.1002/ppp.2031, 2019.

Fleischer, R. L., and Raabe, O.: Recoiling alpha-emitting nuclei. Mechanisms for uranium-series disequilibrium. Geoch. Cosm. Act., 42(7), 973-978. https://doi.org/10.1016/0016-7037(78)90286-7, 1978.

Forman, S. L., Lubinski, D. J., Ingólfsson, Ó., Zeeberg, J. J., Snyder, J. A., Siegert, M. J., and Matishov, G. G.: A review of postglacial emergence on Svalbard, Franz Josef Land and Novaya Zemlya, northern Eurasia. *Quat. Sci. Rev.*, 23(11-13), 1391-1434. https://doi.org/10.1016/j.quascirev.2003.12.007, 2004.

French H.: The Periglacial Environment. Copyright © 2007 by John Wiley & Sons, Ltd., 2007.

French, H.: Recent contributions to the study of past permafrost. Permafr. Periglac. Process, 19(2), 179-194. https://doi.org/10.1002/ppp.614, 2008.

Fu, Z., Wu, Q., Zhang, W., He, H., and Wang, L.: Water Migration and Segregated Ice Formation in Frozen Ground: Current Advances and Future Perspectives. Front. Earth Sci., 10, 826961. https://doi.org/10.3389/feart.2022.826961, 2022.

Gao, Z., Lin, Z., Niu, F., Luo, J., Liu, M., and Yin, G.: Hydrochemistry and controlling mechanism of lakes in permafrost regions along the Qinghai-Tibet Engineering Corridor, China. Geomorphology, 297, 159-169. https://doi.org/10.1016/j.geomorph.2017.09.020, 2017.

Garcia-Solsona, E., Garcia-Orellana, J., Masqué, P., & Dulaiova, H.: Uncertainties associated with 223Ra and 224Ra measurements in water via a Delayed Coincidence Counter (RaDeCC). *Marine Chemistry*, *109*(3-4), 198-219. https://doi.org/10.1016/j.marchem.2007.11.006, 2008

Garcia-Orellana, J., Rodellas, V., Tamborski, J., Diego-Feliu, M., Van Beek, P., Weinstein, Y., Charette, M., Alorda-Kleinglass, A., Michael, H., Stieglitz, T., and Scholten, J.: Radium isotopes as submarine groundwater discharge (SGD) tracers: Review and recommendations. Earth Sci. Rev., 220, 103681. https://doi.org/10.1016/j.earscirev.2021.103681, 2021.

Ghesquière, P., Mineva, T., Talbi, D., Theulè, P., Noble, J.A. and Chiavassa, T.: Diffusion of molecules in the bulk of a low-density amorphous ice from molecular dynamics simulations. Phys. Chem. Chem. Phys. 17, 11455. DOI: 10.1039/c5cp00558b, 2015.

Gilbert, G. L., O'Neill, H. B., Nemec, W., Thiel, C., Christiansen, H. H., and Buylaert, J. P.: Late Quaternary sedimentation and permafrost development in a Svalbard fjord-valley, Norwegian high Arctic. Sedimentology, 65(7), 2531-2558. https://doi.org/10.1111/sed.12476, 2018.

Gilbert, G., Instanes, A., Sinitsyn, A., and Aalberg, A.: Characterization of two sites for geotechnical testing in permafrost: Longyearbyen, Svalbard., AIMS Geosci., 5(4): 868-885. http://hdl.handle.net/11250/2632119, 2019.

Gilichinsky, D., and Wagener, S.: Microbial life in permafrost: A historical review. Permafr. Periglac. Process, 6(3), 243-250. https://doi.org/10.1002/ppp.3430060305, 1995.

Gonneea, M.E., Morris, P.J., Dulaiova, H., and Charette, M.A.: New perspectives on radium behavior within a subterranean estuary. Mar. Chem., 109(3-4), 250–267. https://doi.org/10.1016/j.marchem.2007.12.002, 2008.

Grant, K. M., Rohling, E. J., Ayalon, A., Ramsey, C. B., Satow, C., and Roberts, A. P.: Rapid coupling between ice volume and polar temperature over the past 150,000 years. nature, 491(7426), 744-747. https://doi.org/10.1038/nature11593, 2012.

Grundvåg, S.A., Jelby, M. E., Sliwinska, K.K., Nøhr-Hansen, H., Aadland, T., Sandvik, S. E., Tennvassås, I., Engen, T., and Olaussen, S.: Sedimentology and palynology of the Lower Cretaceous succession of central Spitsbergen: integration of subsurface and outcrop data, Nor. J. Geol., 99, 253–284. https://doi.org/10.17850/njg006, 2019.

Harry, D. G., and Gozdzik, J. S.: Ice wedges: growth, thaw transformation, and palaeoenvironmental significance. J. Quat. Sci., 3(1), 39-55. https://doi.org/10.1002/jqs.3390030107, 1988.

Henkemans, E.: Geochemical Characterization of Groundwaters, Surface Waters and Water-Rock Interaction in an Area of Continuous Permafrost Adjacent to the Greenland Ice Sheet, Kangerlussuaq, Southwest Greenland. A thesis presented to the University of Waterloo, Waterloo, Ontario, Canada. http://hdl.handle.net/10012/10193, 2016.

Herut, B., Starinsky, A., Katz, A., and Bein, A.: The role of seawater freezing in the formation of subsurface brines, Geochim. Cosmochim. Acta., 54, 13–21. https://doi.org/10.1016/0016-7037(90)90190-V, 1990.

Hivon, E. G., and Sego, D. C.: Distribution of saline permafrost in the Northwest Territories, Canada. Can. Geotech. J., 30, 506– 514. https://doi.org/10.1139/t93-043, 1993.

Hodson, A. J., Nowak, A., Hornum, M. T., Senger, K., Redeker, K., Christiansen, H. H., Jessen, S., Betlem, P., Thornton, S. F., Turchyn, A. V., Olaussen, S., and Marca, A.: Sub-permafrost methane seepage from open-system pingos in Svalbard, The Cryosphere, 14, 3829–3842. https://doi.org/10.5194/tc-14-3829-2020, 2020.

Hornum, M. T., Hodson, A. J., Jessen, S., Bense, V., and Senger, K.: Numerical modelling of permafrost spring discharge and open-system pingo formation induced by basal permafrost aggradation. The Cryosphere, 14, 4627–4651. https://doi.org/10.5194/tc-14-4627-2020, 2020.

Hsieh, T., Geibert, W., Stahl, H., Aleynik, D., and Henderson, G. M.: Using the radium quartet (228Ra, 226Ra, 224Ra, and 223Ra) to estimate water mixing and radium inputs in Loch Etive, Scotland. *Limnology and Oceanography*, *58*(3), 1089-1102. https://doi.org/10.4319/lo.2013.58.3.1089, 2013.

Humlum, O., Instanes, A., and Sollid, J. L.: Permafrost in Svalbard: a review of research history, climatic background and engineering challenges. Polar Res, 22(2), 191-215. https://doi.org/10.1111/j.1751-8369.2003.tb00107.x, 2003.

Isaksen, K., Holmlund, P., Sollid, J. L., and Harris, C.: Three deep Alpine-permafrost boreholes in Svalbard and Scandinavia. Permafr. Periglac. Process, 12(1), 13-25. https://doi.org/10.1002/ppp.380, 2001.

Iwahana, G., Cooper, Z. S., Carpenter, S. D., Deming, J. W., and Eicken, H.: Intra-ice and intra-sediment cryopeg brine occurrence in permafrost near Utqiaġvik (Barrow). Permafr. Periglac. Process, 32(3), 427-446. https://doi.org/10.1002/ppp.2101, 2021.

James, M., Lewkowicz, A. G., Smith, S. L., and Miceli, C. M.: Multi-decadal degradation and persistence of permafrost in the Alaska Highway corridor, northwest Canada. Environ. Res. Lett., 8(4), 045013. http://dx.doi.org/10.1088/1748-9326/8/4/045013, 2013.

Jin, H. J., Chang, X. L., and Wang, S. L.: Evolution of permafrost on the Qinghai-Xizang (Tibet) Plateau since the end of the late Pleistocene. J. Geophys., 112(F2). https://doi.org/10.1029/2006JF000521, 2007.

Jones, B. M., Kanevskiy, M. Z., Parsekian, A. D., Bergstedt, H., Ward Jones, M. K., Rangel, R. C., Hinkel, K. M., and Shur, Y.: Rapid Saline Permafrost Thaw Below a Shallow Thermokarst Lake in Arctic Alaska. Geophys. Res. Lett., 50(22), e2023GL105552. https://doi.org/10.1029/2023GL105552, 2023.

Keating, K., Binley, A., Bense, V., Van Dam, R. L., and Christiansen, H. H.: Combined geophysical measurements provide evidence for unfrozen water in permafrost in the Adventdalen valley in Svalbard. Geophys. Res. Lett., 45(15), 7606-7614. https://doi.org/10.1029/2017GL076508, 2018.

Kipp, L. E., Kadko, D. C., Pickart, R. S., Henderson, P. B., Moore, W. S., and Charette, M. A.: Shelf-Basin Interactions and Water Mass Residence Times in the Western Arctic Ocean: Insights Provided by Radium Isotopes. Journal of Geophysical Research: Oceans, 124(5), 3279-3297. https://doi.org/10.1029/2019JC014988, 2019.

Kipp, L., Charette, M., Robbins, A., Pnyushkov, A., Polyakov, I., and Whitmore, L.: Radium Isotopes as Tracers of Shelf-Basin Exchange Processes in the Eastern Arctic Ocean. Journal of Geophysical Research: Oceans, 128(12), e2023JC020303. https://doi.org/10.1029/2023JC020303, 20~~19~~23.

Kipp, L., Chaillou, G., Kienast, M., Tamborski, J., and Whalen, D.: Radon and radium isotope signatures on a massive ice- and permafrost-rich coastline. Geochim. Cosmochim. Acta., *403*, 166-181. https://doi.org/10.1016/j.gca.2025.06.014, 2025.

Kiro, Y., Yechieli, Y., Voss, C.I., Starinsky, A., and Weinstein, Y.: Modeling radium distribution in coastal aquifers during sea level changes: the Dead Sea case. Geochim. Cosmochim. Acta., 88, 237–254. https://doi.org/10.1016/j.gca.2012.03.022, 2012.

Kiro, Y., Weinstein, Y., Starinsky, A., and Yechieli, Y.: Groundwater ages and reaction rates during seawater circulation in the Dead Sea aquifer. Geochim. Cosmochim. Acta., 122, 17-35. https://doi.org/10.1016/j.gca.2013.08.005, 2013.

Kiro, Y., Weinstein, Y., Starinsky, A., and Yechieli, Y.: Application of radon and radium isotopes to groundwater flow dynamics: An example from the Dead Sea. Chem. Geol., 411, 155-171. https://doi.org/10.1016/j.chemgeo.2015.06.014, 2015.

Kraemer, T.F., and Reid, D.F.: The occurrence and behavior of radium in saline formation water of the U.S. Gulf coast region. Isotope Geosci, 2, 153-174. https://doi.org/10.1016/0009-2541(84)90186-4, 1984.

Krishnaswami, S., Graustein, W. C., Turekian, K. K., and Dowd, J. F.: Radium, thorium and radioactive lead isotopes in groundwaters: Application to the in-situ determination of adsorption-desorption rate constants and retardation factors. Water Resour. Res., 18(6), 1663-1675. https://doi.org/10.1029/WR018i006p01663, 1982.

Kumar, A., Rout, S., Pulhani, V. et al.: A review on distribution coefficient (Kd) of some selected radionuclides in soil/sediment over the last three decades. J Radioanal Nucl Chem 323, 13–26 https://doi.org/10.1007/s10967-019-06930-x, 2020

Kwong, Y.T.J., and Gan, T.Y.: Northward migration of permafrost along the Mackenzie highway and climatic warming. Clim. Change, 26, 399–419. https://doi.org/10.1007/BF01094404, 1994.

Lacelle, D., Fisher, D. A., Verret, M., and Pollard, W.: Improved prediction of the vertical distribution of ground ice in Arctic-Antarctic permafrost sediments. Commun. Earth Environ. 3(1), 1-12. https://doi.org/10.1038/s43247-022-00367-z, 2022.

Li, G., Zhang, M., Pei, W., Melnikov, A., Khristoforov, I., Li, R., and Yu, F.: Changes in permafrost extent and active layer thickness in the Northern Hemisphere from 1969 to 2018. Sci. Total Environ., 804, 150182. https://doi.org/10.1016/j.scitotenv.2021.150182, 2022.

Lønne, I. and Nemec, W.: High-arctic fan delta recording deglaciation and environment disequilibrium, Sedimentology, 51, 553–589. https://doi.org/10.1111/j.1365-3091.2004.00636.x, 2004.

Mackay J. R.: Downward water movement into frozen ground, western arctic coast, Canada. Can. J. Earth Sci. 20(1): 120-134. https://doi.org/10.1139/e83-012, 1983.

Mackay, J. R.: Ice-Wedge Cracks, Western Arctic Coast. Can. Geogr., 33(4), 365-368. https://doi.org/10.1111/j.1541-0064.1989.tb00923.x, 1989.

Mackay, J. R., and Dallimore, S. R.: Massive ice of the Tuktoyaktuk area, western Arctic coast, Canada. Can. J. Earth Sci., 29(6), 1235-1249. https://doi.org/10.1139/e92-099, 1992.

Marion, G. M.: Freeze-Thaw Processes and Soil Chemistry (No. CRRELSR9512)., 1995.

Marsh, P., and Woo, M. K.: Infiltration of meltwater into frozen soils in a continuous permafrost environment. In Proceedings of the sixth international conference on permafrost, Vol. 1, pp. 443-448. Beijing: South China University of Technology Press, 1993.

Mathieu, G. G., Biscaye, P. E., Lupton, R. A., and Hammond, D. E.: System for measurement of ^{222}Rn at low levels in natural waters. Health Phys., 55(6), 989-992, 1988.

Moore W. S.: Large groundwater inputs to coastal waters revealed by ^{226}Ra enrichments. Nature, 380, 612–614. https://doi.org/10.1038/380612a0, 1996.

Moore, W. S., and Arnold, R.: Measurement of ^{223}Ra and ^{224}Ra in coastal waters using a delayed coincidence counter. J. Geophys. Res. Oceans, 101(C1), 1321-1329. https://doi.org/10.1029/95JC03139, 1996.

Moore, W.S.: Sources and fluxes of submarine groundwater discharge delineated by radium isotopes. *Biogeochemistry* 66, 75–93, https://doi.org/10.1023/B:BIOG.0000006065.77764.a0, 2003.

Mulrooney, M.J., Larsen, L., Van Stappen, J., Rismyhr, B., Senger, K., Braathen, A., Olaussen, S., Mørk, M.B.E., Ogata, K. and Cnudde, V.: Fluid flow properties of the Wilhelmøya Subgroup, a potential unconventional CO_2 storage unit in central Spitsbergen. Nor. J. Geol. 85-116. https://doi.org/10.17850/njg002, 2018.

Obu, J., Westermann, S., Bartsch, A., et al.: Northern Hemisphere permafrost map based on TTOP modelling for 2000–2016 at 1 km2 scale. Earth-Sci Rev, 193, 299-316. https://doi.org/10.1016/j.earscirev.2019.04.023, 2019.

Ogata, K., Senger, K., Braathen, A., Tveranger, J., and Olaussen, S.: The importance of natural fractures in a tight reservoir for potential CO_2 storage: a case study of the upper Triassic–middle Jurassic Kapp Toscana Group (Spitsbergen, Arctic Norway). Geological Society, London, Special Publications, 374(1), 395-415. https://doi.org/10.1144/SP374.9, 2014.

Opel, T., Meyer, H., Wetterich, S., Laepple, T., Dereviagin, A., and Murton, J. Ice wedges as archives of winter paleoclimate: A review. Permafr. Periglac. Process, 29(3), 199-209. https://doi.org/10.1002/ppp.1980, 2018.

Osterkamp, T. E., and Romanovsky, V. E.: Evidence for warming and thawing of discontinuous permafrost in Alaska. Permafr. Periglac. Process, 10(1), 17-37. https://doi.org/10.1002/(SICI)1099-1530(199901/03)10:1<17::AID-PPP303>3.0.CO;2-4, 1998.

Rama and Moore, W.: Mechanism of transport of U-Th series radioisotopes from solids into ground water. *Geochimica et Cosmochimica Acta*, *48*(2), 395-399. https://doi.org/10.1016/0016-7037(84)90261-8, 1984.

Rotem, D., Lyakhovsky, V., Christiansen, H. H., Harlavan, and Weinstein, Y.: Permafrost saline water and Early to mid-Holocene permafrost aggradation in Svalbard, The Cryosphere, 17, 3363–3381. https://doi.org/10.5194/tc-17-3363-2023, 2023.

Rotem, D., Weinstein, Y., Christiansen, H. H., Sültenfuß, J., and Hodson, A.: Ra isotope perspective on the hydrology and continuity of permafrost in the high Arctic. Sci. Total Environ., 950, 175412. https://doi.org/10.1016/j.scitotenv.2024.175412, 2024.

Rutgers Van Der Loeff, M. M., Key, R. M., Scholten, J., Bauch, D., and Michel, A.: 228Ra as a tracer for shelf water in the Arctic Ocean. Deep Sea Research Part II: Topical Studies in Oceanography, 42(6), 1533-1553. https://doi.org/10.1016/0967-0645(95)00053-4, 1994.

Rutgers van der Loeff, M., Kühne, S., Wahsner, M., Höltzen, H., Frank, M., Ekwurzel, B., Mensch, M., and Rachold, V.: 228Ra and 226Ra in the Kara and Laptev seas. Continental Shelf Research, 23(1), 113-124. https://doi.org/10.1016/S0278-4343(02)00169-3, 2002.

Sheshukov, A. Y., and Nieber, J. L.: One-dimensional freezing of non-heaving unsaturated soils: Model formulation and similarity solution. Water Resour. Res., 47(11). https://doi.org/10.1029/2011WR010512, 2011.

Solomatin, V. I., and Xu, X.: Water migration and ice segregation in the transition zone between thawed and frozen soil. Permafr. Periglac. Process, *5*(3), 185-190. https://doi.org/10.1002/ppp.3430050307, 1994.

Stephani, E., Drage, J., Miller, D., Jones, B. M., and Kanevskiy, M.: Taliks, cryopegs, and permafrost dynamics related to channel migration, Colville River Delta, Alaska. Permafr. Periglac. Process, *31*(2), 239-254. https://doi.org/10.1002/ppp.2046, 2020.

Suksi, J. and Rasilainen, K.: On the Role of α-Recoil in Uranium Migration - Some Findings from the Palmottu natural Analogue Site, SW Finland. Radiochim. Acta, 74(s1), 297-302. https://doi.org/10.1524/ract.1996.74.special-issue.297, 1996.

Sumner, M. E., and Miller, W. P.: Cation exchange capacity and exchange coefficients. In D. L. Sparks et al. (Eds.), Methods of Soil Analysis, Part 3: Chemical Methods (pp. 1201–1229). Soil Science Society of America, Madison, WI., 1996.

Vinson, D.S., Tagma, T., Bouchaou, L., Dwyer, G.S., Warner, N.R., and Vengosh, A.: Occurrence and mobilization of radium in fresh to saline coastal groundwater inferred from geochemical and isotopic tracers (Sr, S, O, H, Ra, Rn). Appl. Geochem. 38 (2013) 161–175. http://dx.doi.org/10.1016/j.apgeochem.2013.09.004, 2013.

Wang, S., Wang, Q., Xu, J., and Ding, J.: Effect of freeze-thaw on freezing point and thermal conductivity of loess. Arab. J. Geosci., 13:206. https://doi.org/10.1007/s12517-020-5186-2, 2020.

Wang, C., Li, S., Lai, Y., Chen, Q., He, X., Zhang, H., and Liu, X.: Predicting the Soil Freezing Characteristic From the Particle Size Distribution Based on Micro-Pore Space Geometry. Water Resour. Res., 58(1), e2021WR030782. https://doi.org/10.1029/2021WR030782, 2021.

Weinstein, Y., Rotem, D., Kooi, H., Yechieli, Y., Sültenfuß, J., Kiro, Y., Harlavan, Y., Feldman, M., and Christiansen, H. H.: Radium isotope fingerprinting of permafrost-applications to thawing and intra-permafrost processes. Permafr. Periglac. Process, 30(2), 104-112. https://doi.org/10.1002/ppp.1999, 2019.

Weinstein, Y., Friedheim, O., Odintsov, L., Harlavan, Y., Nuriel, P., Lazar, B., Burg, A.: Using radium isotopes to constrain the age of saline groundwater, implications to seawater intrusion in aquifers. J. Hydrol., 598, 126412. https://doi.org/10.1016/j.jhydrol.2021.126412, 2021.

Wojtasik, B., Świrydowicz, S., Burska, D., and Nowiński, K.: Radionuclide activities in sediments on the northern coast of Spitsbergen. Polish Polar Research, 291-312. DOI: 10.1515/popore-2017-0019, 2017.

Yershov, E.D.: General Geocryology. English ed. Cambridge, UK: Cambridge University Press.

Zhang, M., Zhang, X., Lu, J., Pei, W., and Wang, C. 2018. Analysis of volumetric unfrozen water contents in freezing soils. Exp. Heat Transf., 32(5), 426–438. https://doi.org/10.1080/08916152.2018.1535528, 1998.